3

Virus transport in the subsurface

Constantinos V. Chrysikopoulos
Department of Civil and Environmental Engineering
University of California, Irvine, CA 92697-2175, USA
E-Mail: costas@eng.uci.edu

Abstract

Mathematical models for virus transport in homogeneous, saturated porous media are presented. All models described in this chapter account for virus sorption and inactivation of liquid phase and adsorbed viruses with different inactivation coefficients. One-dimensional analytical solutions for virus transport in porous media under both constant concentration and constant flux boundary conditions are presented. Furthermore, a numerical one-dimensional virus transport model accounting for time dependent, pseudo first-order inactivation coefficients is introduced. Also, a small perturbation solution to a stochastic model for one-dimensional virus transport accounting for a time dependent distribution coefficient is presented. Subsequently, analytical virus transport models accounting for three-dimensional dispersion within aquifers with infinite, semi-infinite as well as finite thickness under instantaneous and continuous virus loadings from both point and elliptic source geometries are examined. Nonequilibrium reversible virus adsorption which is applicable to viruses behaving as solutes, as well as virus filtration which is suitable for viruses behaving as colloids, are examined. The pseudo first-order approximation is shown to simulate available experimental data better than the constant rate inactivation assumption. Model simulations indicated that a time dependent distribution coefficient results in an enhanced spreading of the liquid phase virus concentration. Moreover, it is demonstrated that the analytical solutions presented for one- and three-dimensional virus transport can successfully simulate available data from field experiments.

1 Introduction

Most of the microorganisms present in groundwater originate from human and animal sewage through municipal wastewater discharges, septic tanks, sanitary landfills and agricultural practices. As microorganisms are released into the subsurface, they infiltrate through the vadose zone, and upon reaching the water table continue to migrate downstream (see Figure 1). Because groundwater is often consumed with inadequate treatment or without any conventional treatment at all, it is necessary to understand fully the mechanisms governing the transport and fate of these microorganisms in groundwater systems so that the health risk due to groundwater pollution by viruses can be evaluated. Mathematical models are frequently used as tools for predicting the movement of viruses in the subsurface and evaluating long-term health risks, by determining safe distances between drinking water wells and sources of contamination (Yates *et al.* [1]).

Viruses are intracellular parasites that can be classified as colloid particles with size ranging from 0.02 μm to 0.3 μm (Brock and Madigan [2]). They are generally negatively charged and vary widely in shape and chemical composition. A virus contains a nucleic acid, either DNA or RNA, which is surrounded by a protein coat (capsid) consisting of a number of protein molecules. These molecules are called capsomeres and they are arranged in a precise and highly repetitive pattern around nucleic acid. Because viruses do not have their own respiratory and biosynthetic functions, they reproduce inside other cells by a process called infection. Viruses are classified on the basis of the hosts they infect. The three major groups of viruses are: animal viruses, plant viruses and bacterial viruses (Brock and Madigan [2]). The most common types of viruses found in groundwater which may infect the human body are animal viruses such as: *adenovirus*, *coliphage*, *coxsackievirus*, *enterovirus*, *hepatitis*, *poliovirus* and *rotavirus* (Gerba and Keswick [3]; Yates and Yates [4]).

The transport and fate of viruses in porous media are mainly governed by virus inactivation and adsorption onto the solid matrix (Vilker [5]). Virus transport in porous media is distinguished from

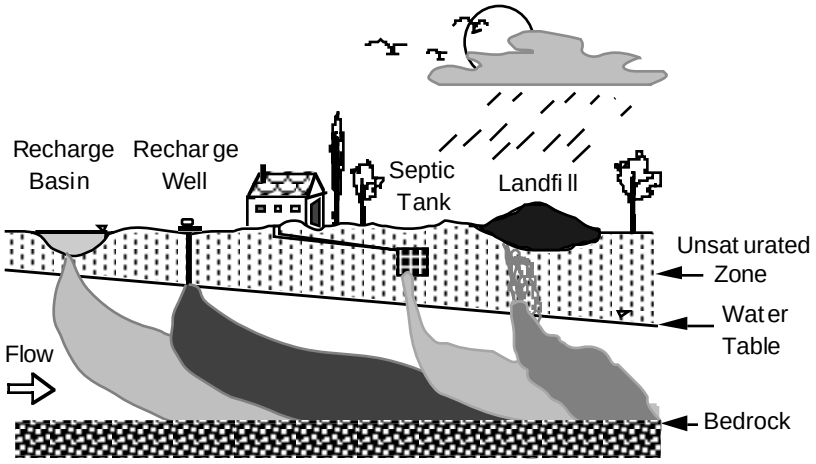

Figure 1. Illustration of sources and patterns of migration of microorganisms in the subsurface

solute transport because viruses undergo considerably different inactivation and adsorption mechanisms. Inactivation of liquid phase as well as sorbed or attached viruses is an irreversible sink mechanism, due to disruption of coat proteins and degradation of the nucleic acid, that is commonly described by a first-order rate expression (Yates and Yates [4]). Unlike the case of solute decay, experimental observations suggest the inactivation rate is smaller for attached than liquid phase viruses (Hurst *et al.* [6], Gerba [7], Yates and Yates [4]). Sobsey *et al.* [8], Gerba [7], and Yates *et al.* [1] indicated that there exists a strong correlation between virus adsorption and inactivation. They showed that virus survival is prolonged for viruses adsorbed onto the solid matrix, because they are protected against disruption of coat protein and degradation of nucleic acid. Thus, inactivation rates of liquid phase and attached viruses should not be assumed equal. The most important factor for virus inactivation in the subsurface is temperature (Yates and Ouyang [9]). Viruses remain infective much longer at lower temperatures (1–8°C) than at higher temperatures (20–32°C) (Park *et al.* [10]). Therefore, near the top layer of an unsaturated subsurface formation where considerable temperature

fluctuations may occur, it is important to account for virus inactivation variation due to temperature fluctuations. Although viruses may undergo sorption via physical adsorption, chemical adsorption or ion exchange in a fashion similar to solute adsorption, the major mechanism of virus attachment results from electrostatic double-layer interactions and van der Waals forces (Teutsch *et al.* [11]). Viruses are larger than dissolved contaminants; however, it should be noted that viruses compose the lower end of the colloid size distribution. For this reason, virus adsorption is often described by either colloid filtration or solute sorption processes. The size of viruses can be an important parameter if the porous medium is highly heterogeneous, where viruses may move faster than conservative tracers (Powelson and Gerba [12]). This phenomenon is known as the pore size exclusion effect, caused by preferential transport of colloids through pores larger than their physical sizes. Consequently, pore size exclusion enhances colloid migration (Gerba *et al.* [13], Powelson *et al.* [14], Abdel-Salam and Chrysikopoulos [15], Chrysikopoulos and Abdel-Salam [16]).

Vilker [5] suggested that the nonequilibrium adsorption process is appropriate for models describing virus transport in porous media, assuming viruses behave as solutes. Nonequilibrium adsorption represents the rate of approach to equilibrium between adsorbed and liquid phase virus concentrations, accounting for virus transport to the outer layer of a solid particle by mass transfer followed by virus immobilization. The colloid filtration theory is frequently employed to models of virus transport in porous media, assuming viruses behave as colloids. Colloids are attached onto the solid matrix through interception, sedimentation (mechanical filtration), and diffusion. The interception and sedimentation processes are effective only for large size particles (≥ 1 μm). Because viruses are of submicron size, for the case of virus filtration, the effects of sedimentation and interception can be neglected (Harvey and Garabedian [17]). For mathematical simplicity, virus adsorption in homogeneous porous media is often described by an equilibrium adsorption relationship assuming an instantaneous equilibrium between viruses in the liquid phase and onto

the solid matrix (Matthess *et al.* [18], Tim and Mostaghimi [19]). For the case of a linear isotherm (linear relationship between the amount of a virus in the liquid phase and sorbed onto the solid matrix) the extent of equilibrium mass partitioning is often reflected by a constant partition coefficient or distribution coefficient, which is equal to the slope of the linear sorption isotherm.

There are only a few mathematical models available in the literature for virus transport in porous media. Grosser [20] employed a one-dimensional advection/dispersion equation to describe virus transport in homogeneous porous media under local equilibrium conditions assuming equal inactivation rates for both adsorbed and liquid phase viruses. Matthess *et al.* [18] presented a model accounting for equilibrium virus adsorption, inactivation, and filtration. Tim and Mostaghimi [19] developed a numerical model for water flow and virus transport in variably saturated formations assuming that virus adsorption is an equilibrium process, and virus inactivation is identical for adsorbed as well as liquid phase viruses. Park *et al.* [10] developed a semi-analytical/numerical model (VIRALT) for both steady-state and transient vertical virus transport in the unsaturated zone and along the flowlines in the saturated zone, accounting for equilibrium adsorption and inactivation. Yates and Ouyang [9] developed a one-dimensional numerical model (VIRTUS) that couples the flow of water, viruses, and heat in unsaturated porous media and accounts for equilibrium adsorption, filtration, and temperature dependent inactivation.

Analytical virus transport models, although limited by many assumptions, are very useful tools for preliminary estimation of virus migration, examination of possible boundary conditions, validation of numerical solutions, and determination of virus transport parameters from laboratory or well defined field experiments. Multidimensional contaminant transport models have several advantages over one-dimensional models. For example, multidimensional models can account for concentration gradients and contaminant transport in directions perpendicular to the groundwater flow. Measuring experimentally lateral and vertical dispersion coefficients is not a trivial

task. However, multidimensional transport models can provide such parameters by direct fitting of available experimental data. In addition, multidimensional models can easily account for a variety of boundary conditions as well as contaminant source geometries.

This chapter provides a collection of one- and three-dimensional mathematical models for virus transport in homogeneous, saturated porous media accounting for nonequilibrium virus sorption and virus inactivation of suspended as well as adsorbed viruses with different inactivation coefficients. Viruses behaving both as solutes and colloids are examined. The impact of time dependent inactivation of suspended as well as adsorbed viruses is investigated. Furthermore, virus adsorption under local equilibrium conditions with a stochastic time dependent distribution coefficient is examined, and the effect of appropriate boundary conditions on one-dimensional virus transport is explored. Subsequently, three-dimensional analytical models of virus transport in aquifers of infinite, semi-infinite as well as finite thickness for a variety of virus source configurations including continuous as well as periodic virus loadings from both point and elliptic source geometries are presented.

2 One-dimensional virus transport models

The one-dimensional virus transport in hydraulically homogeneous, saturated, but geochemically heterogeneous porous media accounting for virus adsorption and inactivation, is governed by the following partial differential equation (Sim and Chrysikopoulos [21])

$$\frac{\partial C(t,x)}{\partial t} + \frac{\rho}{\theta}\frac{\partial C^*(t,x)}{\partial t} = D_x \frac{\partial^2 C(t,x)}{\partial x^2} - U_x \frac{\partial C(t,x)}{\partial x} - \lambda C(t,x) - \lambda^* \frac{\rho}{\theta} C^*(t,x) \qquad (1)$$

where C is the liquid phase virus concentration; C^* is the mass of virus adsorbed on the solid matrix; D_x is the hydrodynamic dispersion coefficient; U_x is the average interstitial velocity; ρ is the bulk density of the solid matrix; λ is the inactivation rate coefficient of

liquid phase viruses; λ^* is the inactivation rate coefficient of sorbed viruses; θ is the porosity of soil medium; and t is time. The left hand side of the preceding equation consists of the virus accumulation terms, and the last two terms on the right hand side represent the inactivation of liquid phase and adsorbed viruses, respectively.

For a one-dimensional, semi-infinite porous medium in the presence of a continuous source of viruses, the appropriate initial and boundary conditions are:

$$C(0,x) = 0 \tag{2}$$

$$C(t,0) = C_\circ \tag{3a}$$

$$-D_x \frac{\partial C(t,0)}{\partial x} + U_x C(t,0) = U_x C_\circ \tag{3b}$$

$$\frac{\partial C(t,\infty)}{\partial x} = 0 \tag{4}$$

where $C_\circ$ is the source concentration. The condition (2) corresponds to the situation where viruses are initially absent from the one-dimensional porous medium. The boundary condition (3a) represents the case of constant concentration at the inlet, while the constant flux boundary condition (3b) implies virus concentration discontinuity at the inlet. The downstream boundary condition (4) preserves concentration continuity for a semi-infinite system.

2.1 Invariant virus inactivation

For the case of constant virus inactivation the rate of virus attachment onto the solid matrix is described by the following generalized expression

$$\frac{\rho}{\theta}\frac{\partial C^*(t,x)}{\partial t} = r_1 C(t,x) - r_2 C^*(t,x) - \lambda^* \frac{\rho}{\theta} C^*(t,x) \tag{5}$$

where r_1 is the forward rate coefficient, and r_2 is the reverse rate coefficient.

The desired expression for C^* is obtained by solving (5) subject to an initial condition of zero sorbed (or filtered) virus concentration ($C^*(0,x)=0$) as

$$C^*(t,x)=\frac{r_1\theta}{\rho}\int_0^t C(\tau,x)\exp\left[-\left(\frac{r_2\theta}{\rho}+\lambda^*\right)(t-\tau)\right]d\tau \qquad (6)$$

where τ is a dummy integration variable. In the view of (5) and (6) the governing equation (1) can be written as

$$\frac{\partial C(t,x)}{\partial t}=D_x\frac{\partial^2 C(t,x)}{\partial x^2}-U_x\frac{\partial C(t,x)}{\partial x}-\mathcal{A}C(t,x)$$
$$-\mathcal{B}\int_0^t C(\tau,x)e^{-\mathcal{H}(t-\tau)}d\tau \qquad (7)$$

where the following substitutions have been employed

$$\mathcal{A}=r_1+\lambda, \qquad \mathcal{B}=\frac{r_1 r_2\theta}{\rho}, \qquad \mathcal{H}=\frac{r_2\theta}{\rho}+\lambda^* \qquad (8a,b,c)$$

2.1.1 Constant concentration boundary condition

For the case of a constant concentration boundary condition, the analytical solution to the governing integrodifferential equation (7) subject to conditions (2), (3a) and (4) is given by (Sim and Chrysikopoulos [21])

$$C_{cc}(t,x)=C_\circ\exp\left[\frac{U_x x}{2D_x}\right]\left\{\int_0^t\mathcal{H}\left(e^{-\mathcal{H}\tau}\int_0^\tau\frac{xJ_o\left[2\left(\mathcal{B}\zeta(\tau-\zeta)\right)^{\frac{1}{2}}\right]}{2\left(D_x\pi\zeta^3\right)^{\frac{1}{2}}}\right.\right.$$
$$\left.\times\exp\left[\frac{-x^2}{4D_x\zeta}+\left(\mathcal{H}-\mathcal{A}-\frac{U_x^2}{4D_x}\right)\zeta\right]d\zeta\right)d\tau$$
$$+e^{-\mathcal{H}t}\int_0^t\frac{xJ_o\left[2\left(\mathcal{B}\zeta(t-\zeta)\right)^{\frac{1}{2}}\right]}{2\left(D_x\pi\zeta^3\right)^{\frac{1}{2}}}$$
$$\left.\times\exp\left[\frac{-x^2}{4D_x\zeta}+\left(\mathcal{H}-\mathcal{A}-\frac{U_x^2}{4D_x}\right)\zeta\right]d\zeta\right\} \qquad (9)$$

where the subscript *cc* indicates the use of the constant concentration upstream boundary condition, J_o is the Bessel function of the first kind of zero order; and ζ is a dummy integration variable.

For the special case of $\lambda = \lambda^* = 0$ using the following substitutions: $r_1\theta/\rho = k_1$, $r_2\theta/\rho = k_2$, $\rho/\theta = 1/\epsilon$, $r_1 = k_1/\epsilon$, and the Bessel function relationship $I_\circ[\eta] = J_\circ[i\eta]$, where $I_\circ$ is the modified Bessel function of the first kind of zero order and η is an arbitrary argument (Abramowitz and Stegun [22]), the analytical solution for the constant concentration boundary condition (9) reduces to the solution presented by Lapidus and Amundson [23]. It should be noted that in the notation of Lapidus and Amundson [23], k_1 and k_2 are the forward and reverse reaction rates, respectively, and ϵ is the fractional void volume.

2.1.2 Constant flux boundary condition

For the case of constant flux boundary condition the analytical solution to the integrodifferential equation (7) subject to conditions (2), (3b) and (4) is given by (Sim and Chrysikopoulos [21])

$$
\begin{aligned}
C_{cf}(t,x) = & \frac{C_\circ U_x}{D_x^{\frac{1}{2}}} \exp\left[\frac{U_x x}{2D_x}\right] \Bigg\{ \int_0^t \int_0^\tau \mathcal{H} e^{-\mathcal{H}\tau} J_o\Big[2\big(\mathcal{B}\zeta(\tau-\zeta)\big)^{\frac{1}{2}}\Big] \\
& \times \Bigg\{ \frac{1}{(\pi\zeta)^{\frac{1}{2}}} \exp\left[\frac{-x^2}{4D_x\zeta} + \left(\mathcal{H} - \mathcal{A} - \frac{U_x^2}{4D_x}\right)\zeta\right] \\
& - \frac{U_x}{2D_x^{\frac{1}{2}}} \exp\left[\frac{U_x x}{2D_x} + \big(\mathcal{H}-\mathcal{A}\big)\zeta\right] \\
& \times \operatorname{erfc}\left[\frac{x}{2\big(D_x\zeta\big)^{\frac{1}{2}}} + \frac{U_x}{2}\left(\frac{\zeta}{D_x}\right)^{\frac{1}{2}}\right] \Bigg\} \, d\zeta \, d\tau \\
& + e^{-\mathcal{H}t} \int_0^t J_o\Big[2\big(\mathcal{B}\zeta(t-\zeta)\big)^{\frac{1}{2}}\Big] \\
& \times \Bigg\{ \frac{1}{(\pi\zeta)^{\frac{1}{2}}} \exp\left[\frac{-x^2}{4D_x\zeta} + \left(\mathcal{H} - \mathcal{A} - \frac{U_x^2}{4D_x}\right)\zeta\right]
\end{aligned}
$$

$$-\frac{U_x}{2D_x^{\frac{1}{2}}}\exp\left[\frac{U_x x}{2D_x}+(\mathcal{H}-\mathcal{A})\zeta\right]$$
$$\times\mathrm{erfc}\left[\frac{x}{2(D_x\zeta)^{\frac{1}{2}}}+\frac{U_x}{2}\left(\frac{\zeta}{D_x}\right)^{\frac{1}{2}}\right]\Bigg\}d\zeta\Bigg\} \tag{10}$$

where the subscript cf indicates the use of the constant flux upstream boundary condition, and $\mathrm{erfc}[\eta] = (2/\pi^{\frac{1}{2}})\int_\eta^\infty e^{-\zeta^2}d\zeta$ is the complimentary error function.

2.1.3 Nonequilibrium adsorption

Assuming that the adsorption process consists of virus diffusion to the outer layer of a solid particle by nonequilibrium mass transfer, and virus immobilization onto the solid particle while in equilibrium with the liquid phase virus concentration in the outer layer, the sorption term in the governing equation (1) can be written as

$$\frac{\rho}{\theta}\frac{\partial C^*(t,x)}{\partial t} = k\big[C(t,x)-C_g(t,x)\big]-\frac{\rho}{\theta}\lambda^* C^*(t,x) \tag{11}$$

where k is the mass transfer rate constant; C_g is the liquid phase virus concentration in direct contact with solids. The parameter C_g can be evaluated from an appropriate isotherm relationship. Vilker [5] suggested the Langmuir isotherm

$$C^*(t,x) = \frac{Q^\circ b^\circ C_g(t,x)}{1+b^\circ C_g(t,x)} \tag{12}$$

where Q° is the Langmuir monolayer capacity, an ultimate solid phase concentration of adsorbed viruses, and b° is a constant related to the bonding energy. Assuming that the liquid phase virus concentration is small or its affinity for the adsorbent is very low ($b^\circ C_g << 1$), the preceding expression reduces to a linear equilibrium relationship

$$C^*(t,x) \simeq Q^\circ b^\circ C_g(t,x) \simeq K_d C_g(t,x) \tag{13}$$

where K_d is the partition or distribution coefficient (liquid volume per solids mass). This assumption is reasonable, and does not limit the virus transport model, because liquid phase virus concentrations present in the subsurface are expected to be relatively low. The preceding relationship is essentially a linear isotherm which does not differ from a Freundlich isotherm with unity exponent.

In the view of (5), (11), and (13) the following substitutions

$$r_1 = k \tag{14}$$

$$r_2 = \frac{k}{Q^\circ b^\circ} \simeq \frac{k}{K_d} \tag{15}$$

can be employed into the general solutions (9) and (10) in order to account for nonequilibrium virus adsorption under constant concentration and constant flux boundary conditions, respectively.

2.1.4 Filtration model

Assuming that the colloid filtration theory is applicable to virus transport, the rate of virus filtration is defined as

$$\frac{\rho}{\theta}\frac{\partial C^*(t,x)}{\partial t} = k_c C(t,x) - \frac{\rho}{\theta}[k_r + \lambda^*]C^*(t,x) \tag{16}$$

where C^* is now the virus concentration retained in the porous medium by the filtration process, and k_c is the clogging rate constant; k_r is the declogging rate constant. The rate of virus filtration depends on the interstitial velocity, suspended virus concentration and filter coefficient. Although colloid filtration is a time dependent process where deposited colloids may alter the surface structure as well as the porosity of the filtering medium and consequently lead to a variable filter coefficient, for the filtration of submicron particles like viruses it is assumed that no change in the filter coefficient occurs progressively in time. The clogging rate constant can be written as

$$k_c = U_x \ \phi \ F(C^*) \tag{17}$$

where ϕ is the filter coefficient, and $F(C^*)$ accounts for variations of porosity with increasing particle attachment. When there is no particle-particle interaction ("clean" media) $F(C^*)$ is assumed to be equal to one.

In view of (5) and (16) it is evident that the following substitutions

$$r_1 = k_c \tag{18}$$

$$r_2 = \frac{k_r \rho}{\theta} \tag{19}$$

can be employed into the general solutions (9) and (10) in order to account for virus filtration under constant concentration and constant flux boundary conditions, respectively.

2.1.5 Model applications

In order to compare the constant concentration and constant flux boundary conditions, breakthrough curves obtained by (9) and (10) for the case of nonequilibrium virus adsorption are plotted in Figure 2 for two different Peclet numbers ($Pe = U_x \ell / D_x$, where ℓ is a characteristic or reference length). The differences in the liquid phase virus concentrations due to the different boundary conditions become negligible with increasing Pe. This result is expected, because by decreasing the hydrodynamic dispersion coefficient and increasing the interstitial velocity the boundary conditions (3a) and (3b) become approximately equivalent.

It has been shown by van Genuchten and Parker [24], Batu and van Genuchten [25], Leij *et al.* [26], and Abdel-Salam and Chrysikopoulos [27] that improper use of boundary conditions may lead to errors in conservation of mass. Assuming that the total virus mass flux entering through the inlet boundary is constant, we can test whether the inlet boundary condition used satisfies mass conservation in the system for the case where mass loss due to inactivation processes is neglected. Following the work of van Genuchten and

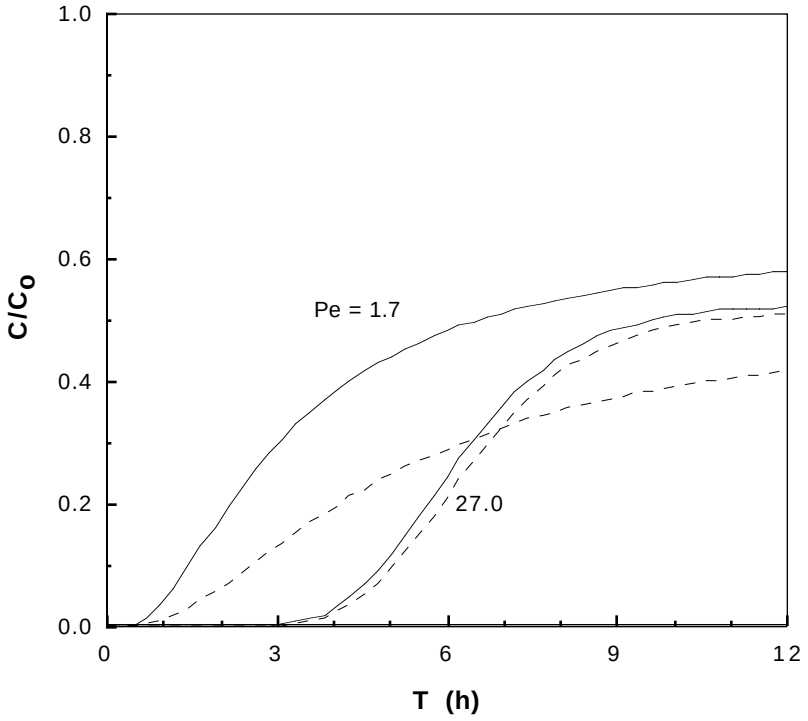

Figure 2. Effect of inlet boundary condition on temporal normalized virus distribution for the case of nonequilibrium adsorption at two different Pe values (here $b^\circ = 1.05\times10^{-11}$ mL/virus, $k = 0.1$ h^{-1}, $\ell = 30$ cm, $Q^\circ = 1.89 \times 10^8$ sites/mg, $\theta = 0.25$, $\lambda = \lambda^* = 0$ d^{-1}, and $\rho = 1.5$ g/cm^3). Solid and dashed lines represent the constant concentration and the constant flux boundary condition, respectively

Parker [24], the relative virus mass balance error, $\mathcal{E}$, can be defined as

$$\begin{aligned}\mathcal{E} &= \mathcal{E}_C + \mathcal{E}_{C^*} - 1 \\ &= \frac{1}{U_x C_\circ t}\int_0^\infty C(t,x)\ dx + \frac{\rho}{\theta U_x C_\circ t}\int_0^\infty C^*(t,x)\ dx - 1 \end{aligned} \qquad (20)$$

where the term $U_x C_\circ t$ is the mass of viruses entering the system at the inlet boundary over the time period t, and the integrals on

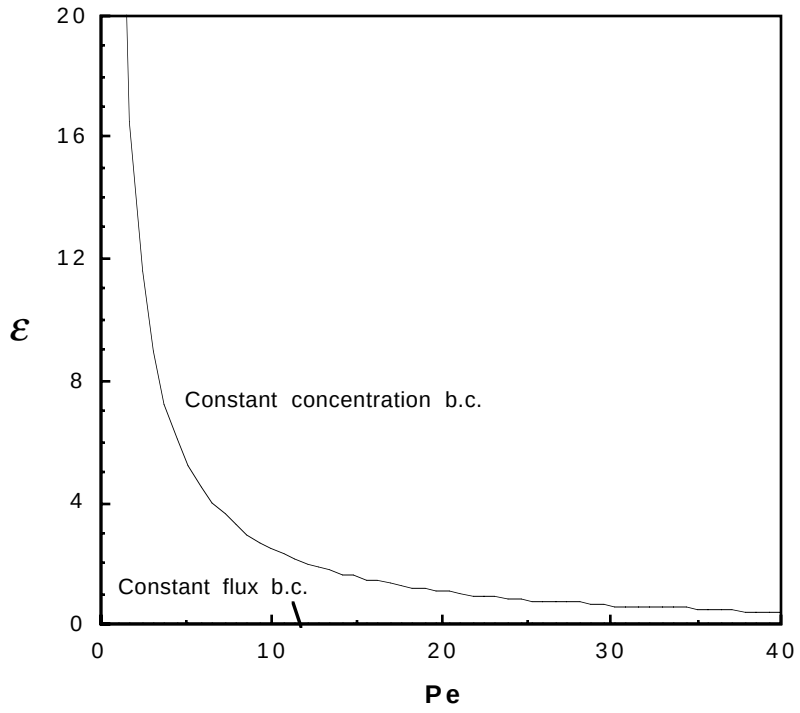

Figure 3. Relative mass error evaluated for the case of nonequilibrium virus adsorption under constant flux and constant concentration boundary conditions as a function of Pe (here $b = 1.05 \times 10^{-11}$ mL/virus, $k = 0.01$ h^{-1}, $\ell = 10$ m, $Q^{\circ} = 1.89 \times 10^{8}$ sites/mg, $t = 240$ h, $\theta = 0.25$, $\lambda = \lambda^{*} = 0$ d^{-1}, and $\rho = 1.5$ g/cm^{3})

the right hand side of the preceding equation represent the mass of viruses suspended in solution and deposited onto the solid matrix, respectively, present in the system at time t. In view of (6), the integral expression for the deposited virus concentration in (20) can be written as

$$\mathcal{E}_{C^*} = \frac{r_1}{U_x C_\circ t} \int_0^{\infty} \int_0^{t} C(\tau, x) \exp\left[-\frac{r_2 \theta}{\rho}(t-\tau)\right] d\tau \; dx \qquad (21)$$

The total relative mass errors for the two boundary conditions as a function of Peclet number are shown in Figure 3. Clearly, the

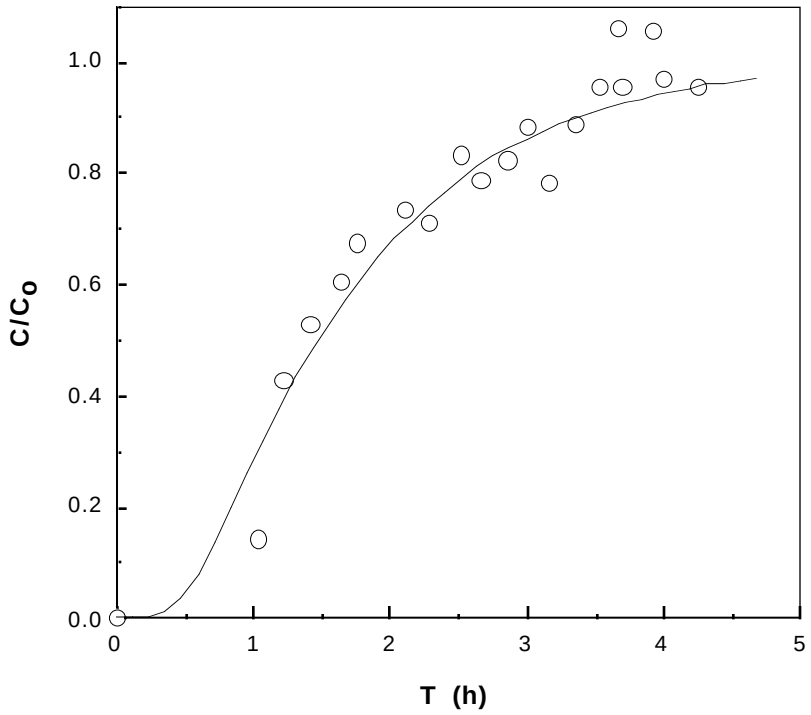

Figure 4. Normalized bacteriophage *MS-2* breakthrough concentrations from column experiments conducted by Bales *et al.* [28] (open circles) and simulated concentration history (solid curve)

relative mass balance error for the constant concentration boundary condition is minimized with increasing Pe. Consequently, the discrepancies in the normalized concentrations between the two boundary conditions presented in Figure 2 can be attributed to this relative mass balance error caused by the constant concentration boundary condition.

The general solution for the case of constant flux boundary condition (10) was evaluated by simulating the bacteriophage *MS-2* breakthrough response from the second column experiment published by Bales *et al.* [28]. The unknown parameters were obtained by a nonlinear least square regression method (Kahaner *et al.* [29]). Given that for the particular experimental data set $\theta = 0.35$, $\rho = 1.6$ g/cm^3,

and $U_x = 13.32$ cm/h, the estimated parameters are: $D_x = 31.75$ cm^2/h, $r_1 = 0.79$ h^{-1}, $r_2 = 9.58$ g/mL·h, and $\lambda = \lambda^* \simeq 0$. The estimated values of the inactivation rate constants were expected to be approximately zero because the experiment was run at 4°C in order to eliminate viral inactivation (Bales *et al.* [28]). For the nonequilibrium adsorption case, in view of (14) and (15), $k = 0.79$ h^{-1} and $Q^\circ b = 8.27 \times 10^{-5}$ mL/mg. For the case of virus filtration, in view of (18) and (19), $k_c = 0.79$ h^{-1} and $k_r = 2.09$ h^{-1}. The experimental data together with the model simulated profile are shown in Figure 4. Good agreement between the experimental data and the simulated concentration history is shown.

2.2 Time-dependent virus inactivation

Temporal variation of inactivation rate coefficients due to variabilities of virus characteristics has been observed in several experimental studies. Parkinson and Huskey [30] and Pollard and Solosko [31] noticed that bacteriophage λ and T_4 populations consist of two subpopulations with different resistance to heat (biphasic inactivation). They observed that the most sensitive viruses inactivate rapidly, while the remaining more resistant viruses undergo slower inactivation. Similarly, Yamagishi and Ozeki [32] reported that the inactivation of bacteriophage λ exhibits two or more distinct phases (multiphasic inactivation), corresponding to subpopulations undergoing sequential inactivation with different inactivation rate coefficients. Grant *et al.* [33] also observed multiphasic sequential inactivation of bacteriophage λ during batch experiments with and without the presence of sand.

Traditionally, models for virus transport through porous formations assume that the inactivation rate coefficients are constant (Yates and Ouyang [9], Chrysikopoulos and Sim [34]). It should be noted, however, that sequential inactivation of a virus population requires two or more discrete first-order rate coefficients, each governing a different inactivation phase (Crane and Moore [35]). For

mathematical simplicity, the multiphasic sequential inactivation can be approximated by a pseudo first-order expression with a time dependent inactivation rate coefficient.

Sim and Chrysikopoulos [36] introduced a model for one-dimensional virus transport in homogeneous, saturated porous media accounting for virus sorption and inactivation with time dependent rate coefficients. The inactivation process is represented by a pseudo first-order expression with time dependent rate coefficients determined from available experimental data. Consequently, the inactivation of viruses in the liquid phase and solid phase are described by the following modified first-order rate expressions

$$\frac{dC(t)}{dt} = -\lambda(t)C(t) \tag{22}$$

$$\frac{dC^*(t)}{dt} = -\lambda^*(t)C^*(t) \tag{23}$$

respectively, where the time dependent inactivation rate coefficients of viruses in the respective phases are described by

$$\lambda(t) = \lambda_\circ e^{-\alpha t} \tag{24}$$

$$\lambda^*(t) = \lambda^*_\circ e^{-\alpha^* t} \tag{25}$$

where $\lambda_\circ$ and $\lambda^*_\circ$ are the initial inactivation rate coefficients of viruses in the respective phases; and α and α^* are the resistivity coefficients of viruses in the respective phases. The magnitude of α is proportional to the resistivity of the dominant subpopulation, because the overall inactivation is controlled by the dominant subpopulation. The initial inactivation rate coefficients of viruses in the liquid phase are assumed to be twice as large as the coefficients of adsorbed viruses ($\lambda^*_\circ = \lambda_\circ/2$) (Reddy *et al.* [37], Yates and Ouyang [9]). Furthermore, the resistivity coefficient of adsorbed viruses is considered to be equal to the resistivity coefficient of viruses in the liquid phase ($\alpha^* = \alpha$). Substituting (24) into (22) and solving the resulting expression subject to the initial condition $C(0) = C_i$, where C_i is the initial liquid phase virus concentration, yields

$$\ln\left[\frac{C(t)}{C_i}\right] = \frac{\lambda_\circ}{\alpha}\left(e^{-\alpha t} - 1\right) \tag{26}$$

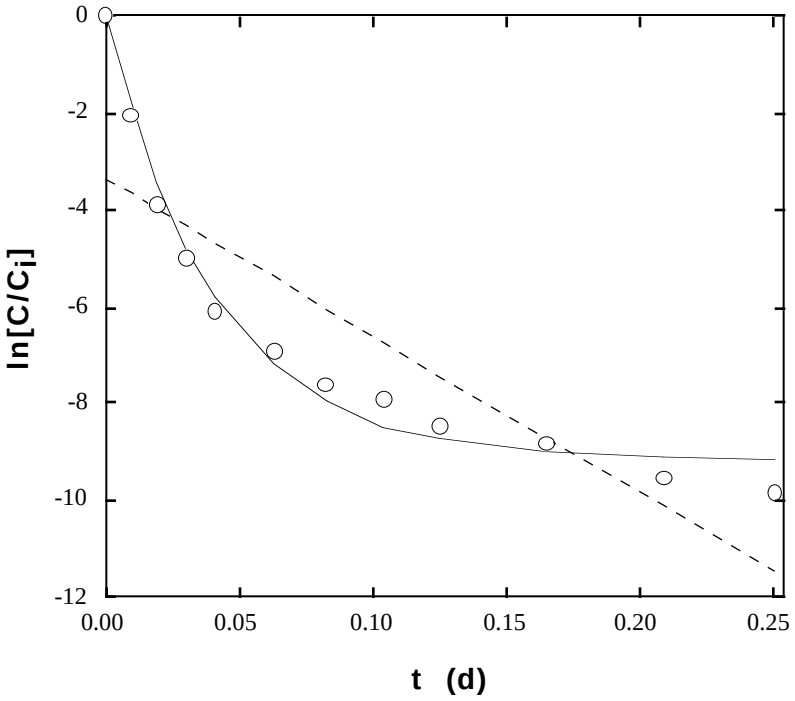

Figure 5. Batch inactivation experimental data (circles) for bacteriophage λ^{++} at 60°C with 10 mM $MgSO_4$ under aerobic conditions adopted from Parkinson and Huskey [30], and simulated concentration history based on the pseudo first-order inactivation model (solid curves) and constant rate inactivation model (dashed lines)

The parameters $\lambda_\circ$ and α can be obtained by fitting the preceding equation to existing experimental data.

Figure 5 presents bacteriophage λ^{++} inactivation experimental data collected by Parkinson and Huskey [30] fitted by both (26) and the constant inactivation rate model ($\lambda(t) = \lambda$). The estimated parameters for the time dependent inactivation model are $\lambda_\circ = 226.02$ d^{-1}, $\alpha = 24.65$ d^{-1} and the corresponding residual sums of squared error (sse) is 1.67; whereas for the constant inactivation model $\lambda = 32.28$ d^{-1} and $sse = 26.71$. It is evident from Figure 5 that the pseudo first-order inactivation rate model simulates

the experimental data much better than the constant inactivation rate model, which fails to match the data at early and late times. The slope of the tangent to a point of the solid curve represents the inactivation rate coefficient at the particular time.

The effect of temporally variable inactivation on liquid phase virus concentration in saturated porous media is illustrated by the model simulations presented in Figure 6. The governing virus transport equation (1) in conjunction with the relationships (11), (13), (24), and (25) is solved numerically subject to initial/boundary conditions (2), (3b), and (4). The numerical solution is obtained by using the IMSL one-dimensional partial differential equation solver MOLCH (IMSL [38]). Figure 6 indicates that, early on, the simulated concentration profile for the case of pseudo first-order inactivation is lower than the one for the case of constant inactivation rate (Figure 6a), whereas at late time the concentration levels are reversed (Figure 6b). The temporally variable inactivation allows rapid inactivation of the most sensitive subpopulations at an early time, and extended survival of the most resistive subpopulations at a later time. Therefore, viruses may remain infective in porous media for an extended period of time and thus travel farther downstream from the source.

2.3 Virus sorption with time dependent distribution coefficient

Recent investigations suggest that the distribution coefficient for a contaminant in a physicochemically heterogeneous subsurface formation is not constant but exhibits temporal as well as spatial variability (Durant and Roberts [39], Bosma *et al.* [40], Smith *et al.* [41]). Excluding the possibilities of mass transport limitations and solute transformation, this variability may be attributed to many factors, including grain size and surface area of adsorbent, chemical composition of groundwater, pH, redox potential, temperature, and solid to liquid ratio (Moody [42]). Proteins (primary constituents of viruses) are also known to exhibit sorption variations with fluctuating external conditions (Norde [44]). In principle, the results obtained from

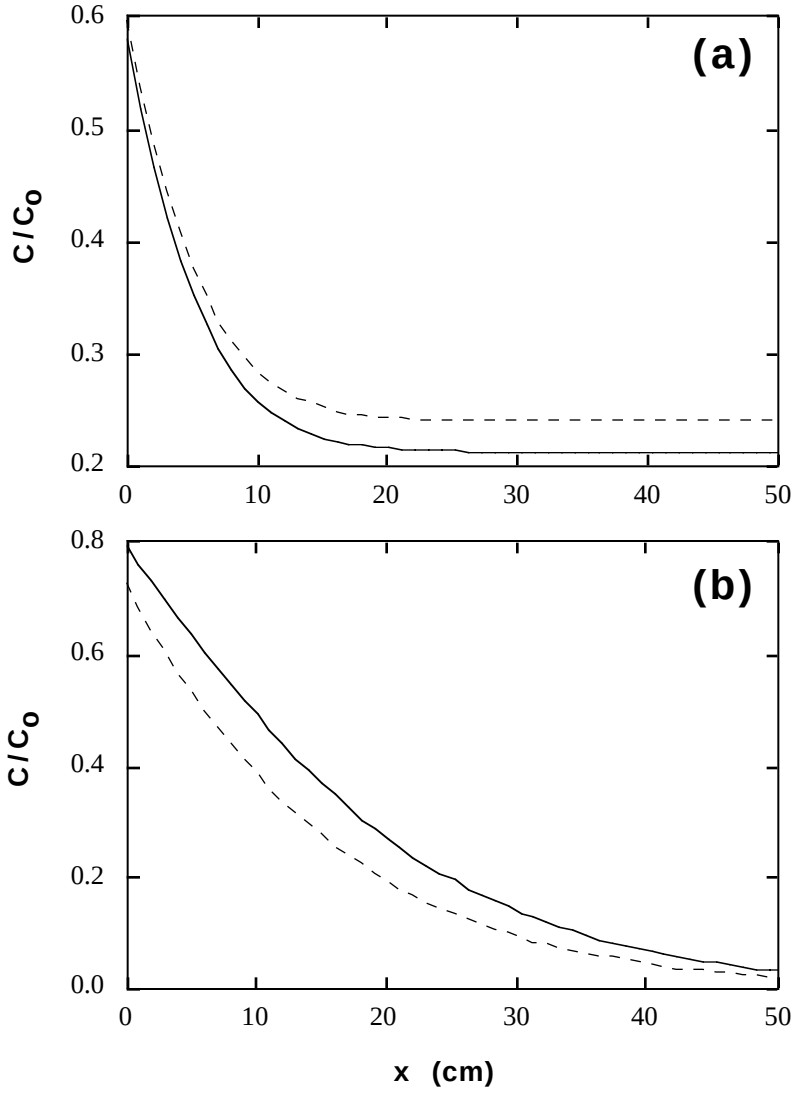

Figure 6. Liquid phase virus concentration snapshots for pseudo first-order (solid curves) or constant rate (dashed curves) inactivation at (a) t=0.05 d and (b) t=10 d (here $D_x = 32.04$ cm^2/h, $U_x = 5.04$ cm/h (Bales *et al.* [28]); $K_d = 2.08 \times 10^{-2}$ ml/mg (Vilker [5]); $k = 1.2$ h^{-1} (Vilker and Burge [43]); $\rho = 1.5$ g/cm^3 (Yates and Ouyang [9]); and $\theta = 0.25$ (Park *et al.* [10]); $\lambda_\circ = 2.66$ d^{-1} and $\alpha = 2.41$ d^{-1})

solutes and proteins can be extended to viruses. Therefore, it is reasonable to consider virus adsorption as a time dependent process, and consequently the distribution coefficient a time dependent parameter.

Chrysikopoulos and Sim [34] developed an analytical virus transport model accounting for virus inactivation and linear local equilibrium adsorption with a stochastic time dependent distribution coefficient. The model assumes that the time dependent local equilibrium virus adsorption is expressed as

$$C^*(t,x) = K_d(t)C(t,x) \tag{27}$$

where $K_d(t)$ is the time dependent distribution coefficient. Consequently,

$$\frac{\partial C^*(t,x)}{\partial t} = C(t,x)\frac{\partial K_d(t)}{\partial t} + K_d(t)\frac{\partial C(t,x)}{\partial t} \tag{28}$$

and the governing one-dimensional virus transport equation (1) is written as

$$\left[1+\frac{\rho}{\theta}K_d(t)\right]\frac{\partial C(t,x)}{\partial t} + C(t,x)\frac{\rho}{\theta}\frac{\partial K_d(t)}{\partial t} = D_x\frac{\partial^2 C(t,x)}{\partial x^2} - U_x\frac{\partial C(t,x)}{\partial x} - \lambda C(t,x) - \lambda^*\frac{\rho}{\theta}K_d(t)C(t,x) \tag{29}$$

The distribution coefficient and, consequently, the virus concentration are assumed to be stochastic processes. The stochastic distribution coefficient is stationary with mean $\langle K_d\rangle = E[K_d(t)]$, where the angle brackets signify ensemble average or expected value over time of a random process, whereas the concentration is both nonstationary and space dependent. The liquid phase virus concentration and the time dependent distribution coefficient are expressed as

$$C(t,x) = \langle C\rangle(t,x) + C'(t,x) \tag{30}$$

$$K_d(t) = \langle K_d\rangle + K_d'(t) \tag{31}$$

where $\langle C\rangle(t,x)$ is the concentration mean, the prime signifies fluctuations in time, $E\big[C'(t,x)\big] = E\big[K_d'(t)\big] = 0$. The analytical solution to (29) subject to initial and boundary conditions (2), (3b), and (4) was derived by Chrysikopoulos and Sim [34] by the method of small perturbation or first-order approximation and is expressed as

$$\langle C\rangle(t,x) = \int_0^t d\tau \int_0^\infty F(t-\tau,x,\xi)\psi(\tau,\xi)\ d\xi + \int_0^t F(t-\tau,x,0)\gamma(\tau,0)\ d\tau \tag{32}$$

where ξ is a dummy integration variable,

$$\psi(t,x) = \frac{-\mathcal{G}(t,x)}{\left[1+\dfrac{\rho}{\theta}\langle K_d\rangle\right]} \tag{33}$$

$$\gamma(t,0) = \frac{U_x C_\circ}{\left[1+\dfrac{\rho}{\theta}\langle K_d\rangle\right]} \tag{34}$$

$$\begin{aligned} F(t,x,\xi) = {} & \left(\frac{1}{4\widehat{D}_x\pi t}\right)^{\frac{1}{2}} \exp\left[\frac{\widehat{U}_x(x-\xi)}{2\widehat{D}_x} - \frac{(x-\xi)^2}{4\widehat{D}_x t} - \left(\widehat{\lambda}+\frac{\widehat{U}_x^2}{4\widehat{D}_x}\right)t\right] \\ & + \left(\frac{1}{4\widehat{D}_x\pi t}\right)^{\frac{1}{2}} \exp\left[\frac{\widehat{U}_x(x-\xi)}{2\widehat{D}_x} - \frac{\big(x+\xi\big)^2}{4\widehat{D}_x t} - \left(\widehat{\lambda}+\frac{\widehat{U}_x^2}{4\widehat{D}_x}\right)t\right] \\ & - \left(\frac{\widehat{U}_x}{2\widehat{D}_x}\right) \exp\left[\frac{\widehat{U}_x x}{\widehat{D}_x} - \widehat{\lambda}t\right] \operatorname{erfc}\left[\left(\frac{\widehat{U}_x^2 t}{4\widehat{D}_x}\right)^{\frac{1}{2}} + \frac{x+\xi}{\big(4\widehat{D}_x t\big)^{\frac{1}{2}}}\right] \end{aligned} \tag{35}$$

$$\widehat{D}_x = \frac{D_x}{\left[1+\dfrac{\rho}{\theta}\langle K_d\rangle\right]} \tag{36}$$

$$\widehat{U}_x = \frac{U_x}{\left[1+\dfrac{\rho}{\theta}\langle K_d\rangle\right]} \tag{37}$$

$$\widehat{\lambda} = \frac{\left[\lambda + \lambda^* \frac{\rho}{\theta}\langle K_d\rangle\right]}{\left[1 + \frac{\rho}{\theta}\langle K_d\rangle\right]} \tag{38}$$

$$\mathcal{G}(t,x) = A(t,x) + B(t,x) + H(t,x) \tag{39}$$

$$A(t,x) = \frac{\rho}{\theta}\int_0^t d\tau \int_0^\infty \frac{\partial F(t-\tau,x,\xi)}{\partial t} Q_1(t,\tau,\xi)\ d\xi - \frac{\rho}{\theta} Q_1(t,t,x) \tag{40}$$

$$B(t,x) = -\frac{\rho}{\theta}\int_0^t d\tau \int_0^\infty F(t-\tau,x,\xi) Q_2(t,\tau,\xi)\ d\xi \tag{41}$$

$$H(t,x) = \frac{\rho}{\theta}\lambda^* \int_0^t d\tau \int_0^\infty F(t-\tau,x,\xi) Q_1(t,\tau,\xi)\ d\xi \tag{42}$$

$$\begin{aligned} Q_1(t,\tau,\xi) = &-\frac{\rho}{\theta}\left[1 + \frac{\rho}{\theta}\langle K_d\rangle\right]^{-1} \left\{ \frac{\partial \langle C_0\rangle(\tau,\xi)}{\partial \tau} E\left[K_d'(t) K_d'(\tau)\right] \right. \\ &+ \langle C_0\rangle(\tau,\xi) E\left[K_d'(t)\frac{\partial K_d'(\tau)}{\partial \tau}\right] \\ &\left. + \lambda^* \langle C_0\rangle(\tau,\xi) E\left[K_d'(t) K_d'(\tau)\right] \right\} \end{aligned} \tag{43}$$

$$\begin{aligned} Q_2(t,\tau,\xi) = &-\frac{\rho}{\theta}\left[1 + \frac{\rho}{\theta}\langle K_d\rangle\right]^{-1} \left\{ \frac{\partial \langle C_0\rangle(\tau,\xi)}{\partial \tau} E\left[\frac{\partial K_d'(t)}{\partial t} K_d'(\tau)\right] \right. \\ &+ \langle C_0\rangle(\tau,\xi) E\left[\frac{\partial K_d'(t)}{\partial t}\frac{\partial K_d'(\tau)}{\partial \tau}\right] \\ &\left. + \lambda^* \langle C_0\rangle(\tau,\xi) E\left[\frac{\partial K_d'(t)}{\partial t} K_d'(\tau)\right] \right\} \end{aligned} \tag{44}$$

$$\begin{aligned} \langle C_0\rangle(t,x) = C_\circ \Bigg\{ &\left[\frac{U_x}{U_x + \kappa}\right] \exp\left[\frac{x\left(U_x - \kappa\right)}{2D_x}\right] \operatorname{erfc}\left[\frac{x\Lambda - \kappa t}{2\left(D_x \Lambda t\right)^{\frac{1}{2}}}\right] \\ &+ \left[\frac{U_x}{U_x - \kappa}\right] \exp\left[\frac{x\left(U_x + \kappa\right)}{2D_x}\right] \operatorname{erfc}\left[\frac{x\Lambda + \kappa t}{2\left(D\Lambda t\right)^{\frac{1}{2}}}\right] \\ &+ \left[\frac{U_x^2}{2D_x\omega}\right] \exp\left[\frac{U_x x}{D_x} - \frac{\omega t}{\Lambda}\right] \operatorname{erfc}\left[\frac{x\Lambda + U_x t}{2\left(D_x \Lambda t\right)^{\frac{1}{2}}}\right] \Bigg\} \end{aligned} \tag{45}$$

$$\kappa = \left(U_x^2 + 4D_x\omega\right)^{\frac{1}{2}} \tag{46}$$

$$\omega = \lambda + \lambda^* \frac{\rho}{\theta}\langle K_d\rangle \tag{47}$$

$$\Lambda = 1 + \frac{\rho}{\theta}\langle K_d\rangle \tag{48}$$

$$\begin{aligned}
\frac{\partial\langle C_0\rangle(t,x)}{\partial t} = C_\circ \Bigg\{ & \left[\frac{U_x}{U_x+\kappa}\right]\left[\frac{x\Lambda+\kappa t}{2\left(D\Lambda\pi t^3\right)^{\frac{1}{2}}}\right] \\
& \times \exp\left[\frac{x\left(U_x-\kappa\right)}{2D_x}\right]\exp\left[\frac{-\left(x\Lambda-\kappa t\right)^2}{4D_x\Lambda t}\right] \\
& + \left[\frac{U_x}{U_x-\kappa}\right]\left[\frac{x\Lambda-\kappa t}{2\left(D_x\Lambda\pi t^3\right)^{\frac{1}{2}}}\right] \\
& \times \exp\left[\frac{x\left(U_x+\kappa\right)}{2D_x}\right]\exp\left[\frac{-\left(x\Lambda+\kappa t\right)^2}{4D_x\Lambda t}\right] \\
& + \left[\frac{U_x^2}{2D_x\omega}\right]\left[\frac{x\Lambda-U_x t}{2\left(D_x\Lambda\pi t^3\right)^{\frac{1}{2}}}\right] \\
& \times \exp\left[\frac{U_x x}{D_x}-\frac{\omega t}{\Lambda}\right]\exp\left[\frac{-\left(x\Lambda+U_x t\right)^2}{4D_x\Lambda t}\right] \\
& - \left[\frac{U_x^2}{2D_x\Lambda}\right]\exp\left[\frac{U_x x}{D_x}-\frac{\omega t}{\Lambda}\right]\operatorname{erfc}\left[\frac{x\Lambda+U_x t}{2\left(D_x\Lambda t\right)^{\frac{1}{2}}}\right]\Bigg\}
\end{aligned} \tag{49}$$

It should be noted that the derived solution is quite general because no assumptions are made about the time-dependent autocovariance function of the distribution coefficient fluctuations about its mean value. However, the frequently employed exponential autocovariance function (e.g. Agterberg [45], Chrysikopoulos *et al.* [46], Bellin *et al.* [47]) is assumed to characterize the fluctuations of $K_d'(t)$, and is defined as (Chrysikopoulos and Sim [34])

$$E\left[K_d'(t)K_d'(\tau)\right] = \sigma_{K_d'}^2 \exp\left[\frac{-(t-\tau)}{a_t}\right] \qquad (t \geq \tau) \tag{50}$$

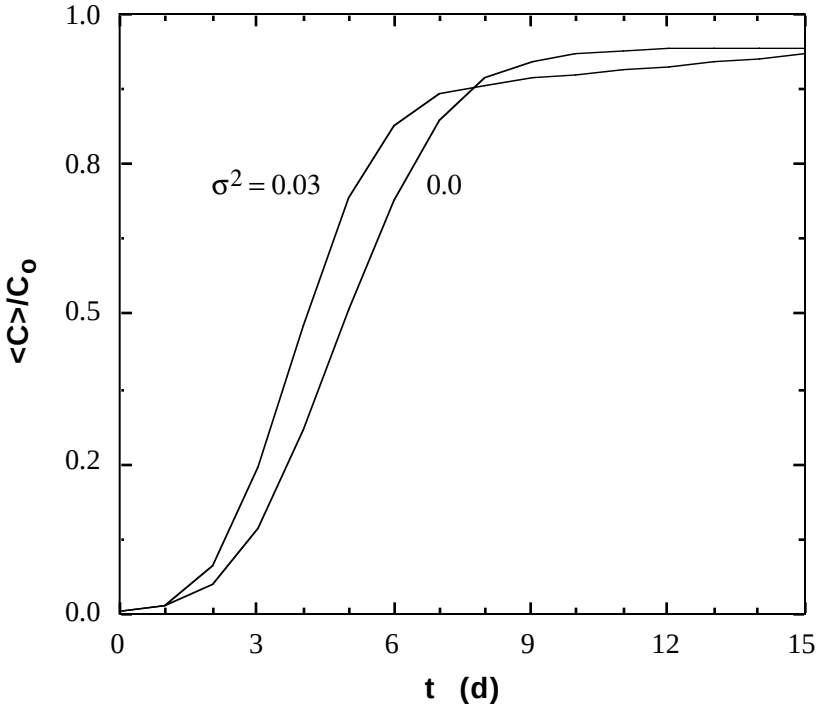

Figure 7. Effect of the time dependent distribution coefficient on temporal ensemble average normalized liquid phase virus concentration profiles for two different variances of the fluctuating distribution coefficient (here $D_x = 1.6$ cm^2/h, $U_x = 1.0$ cm/h, $a_t = 0.5$ d, $\langle K_d \rangle = 0.33$ g/cm^3, $\lambda = 0.03$ d^{-1}, $\lambda^* = 0.003$ d^{-1}, $\theta = 0.25$, and $\rho = 1.5$ g/cm^3)

where $\sigma^2_{K'_d}$ is the variance of $K'_d(t)$, and a_t is the time correlation scale of $K'_d(t)$. In view of (50) the remaining three covariance functions present in (43) and (44) are evaluated as

$$E\left[K'_d(t)\frac{\partial K'_d(\tau)}{\partial \tau}\right] = \frac{1}{a_t} E\left[K'_d(t)K'_d(\tau)\right] \tag{51}$$

$$E\left[\frac{\partial K'_d(t)}{\partial t}K'_d(\tau)\right] = -\frac{1}{a_t} E\left[K'_d(t)K'_d(\tau)\right] \tag{52}$$

$$E\left[\frac{\partial K_d'(t)}{\partial t}\frac{\partial K_d'(\tau)}{\partial \tau}\right] = -\frac{1}{a_t^2}E\left[K_d'(t)K_d'(\tau)\right] \tag{53}$$

Breakthrough curves created by the stochastic virus transport model (32) and the constant distribution coefficient ($K_d(t) = K_d$) model are presented in Figure 7. Two different variances for $K_d'(t)$ are considered, including the zero-variance which corresponds to the situation where the distribution coefficient is constant. It is shown that the temporally variable distribution coefficient leads to earlier breakthrough and enhanced spreading of the ensemble average liquid phase virus concentration. The broadening of the predicted ensemble average liquid phase virus concentration curves can also be interpreted as the result of an effective increase in the dispersive mass flux caused by the time dependent distribution coefficient. This observation is analogous to the enhancement of solute spreading caused by a spatially variable retardation factor (Chrysikopoulos *et al.* [46]).

3 Three-dimensional models for virus transport

The transport of viruses in saturated, homogeneous porous media, accounting for three-dimensional hydrodynamic dispersion in a uniform flow field, virus adsorption, and first-order inactivation of liquid phase and deposited viruses with different inactivation rate coefficients, is governed by the following partial differential equation (Sim and Chrysikopoulos [48])

$$\begin{aligned}\frac{\partial C(t,x,y,z)}{\partial t} + \frac{\rho}{\theta}\frac{\partial C^*(t,x,y,z)}{\partial t} - D_x\frac{\partial^2 C(t,x,y,z)}{\partial x^2} \\ - D_y\frac{\partial^2 C(t,x,y,z)}{\partial y^2} - D_z\frac{\partial^2 C(t,x,y,z)}{\partial z^2} \\ + U_x\frac{\partial C(t,x,y,z)}{\partial x} + \lambda C(t,x,y,z) \\ + \lambda^*\frac{\rho}{\theta}C^*(t,x,y,z) = S(t,x,y,z)\end{aligned} \tag{54}$$

where D_y, and D_z are the lateral, and vertical hydrodynamic dispersion coefficients, respectively; y, and z are the spatial coordinates in the lateral, and vertical directions, respectively; and S is a general form of the virus source configuration. The first two terms on the left-hand side of the preceding equation are accumulation terms, whereas the last two terms on the left-hand side represent the inactivation of liquid phase and deposited viruses, respectively.

In view of the three-dimensional version of (5) and (6) the governing virus transport equation (54) is written as

$$\begin{aligned}\frac{\partial C(t,x,y,z)}{\partial t} &- D_x\frac{\partial^2 C(t,x,y,z)}{\partial x^2} - D_y\frac{\partial^2 C(t,x,y,z)}{\partial y^2} \\ &- D_z\frac{\partial^2 C(t,x,y,z)}{\partial z^2} + U_x\frac{\partial C(t,x,y,z)}{\partial x} \\ &+ \mathcal{A}C(t,x,y,z) - \mathcal{B}\int_0^t C(\tau,x,y,z)e^{-\mathcal{H}(t-\tau)}d\tau \\ &= S(t,x,y,z) \end{aligned} \tag{55}$$

The virus source configuration is represented by the following general function

$$S(t,x,y,z) = G(t)\ W(x,y,z) \tag{56}$$

where $G(t)$ is the virus mass release rate from the source, and the function $W(x,y,z)$ signifies the inverse of the source volume from which the virus mass is introduced into a porous medium. It should be noted, however, that $G(t)$ characterizes the source loading type. In this work, instantaneous as well as continuous or temporally periodic source loading functions are considered. Furthermore, $W(x,y,z)$ characterizes the source physical geometry.

3.1 Infinite porous medium with a point source

The appropriate initial and boundary conditions for an infinite three-dimensional porous medium are:

$$C(0,x,y,z) = C^*(0,x,y,z) = 0 \tag{57}$$

$$C(t, \pm\infty, y, z) = 0 \tag{58}$$

$$C(t, x, \pm\infty, z) = 0 \tag{59}$$

$$C(t, x, y, \pm\infty) = 0 \tag{60}$$

The analytical solution to (55) subject to conditions (57)-(60) has been derived by Sim and Chrysikopoulos [48] and is expressed as

$$\begin{aligned} C(t,x,y,z) = & \left(\frac{1}{16\pi^2 D_x D_y}\right)^{\frac{1}{2}} \int_0^t \int_{-\infty}^{\infty} \int_{-\infty}^{\infty} \int_{-\infty}^{\infty} \exp\left[\frac{U_x(x-q)}{2D_x}\right] \\ & \times S(t-\tau, q, v, p)\Bigg[\mathcal{H}Q(\tau, x-q, y-v, z-p) \\ & + \frac{\partial Q(\tau, x-q, y-v, z-p)}{\partial \tau}\Bigg] dp\ dv\ dq\ d\tau \end{aligned} \tag{61}$$

where

$$\begin{aligned} Q(t,x,y,z) = & e^{-\mathcal{H}t} \int_0^t I_\circ\left[2\left(\mathcal{B}\zeta(t-\zeta)\right)^{\frac{1}{2}}\right] \left(\frac{1}{4\pi D_z \zeta^3}\right)^{\frac{1}{2}} \\ & \times \exp\Bigg[-\frac{1}{4\zeta}\left(\frac{x^2}{D_x} + \frac{y^2}{D_y} + \frac{z^2}{D_z}\right) \\ & - \zeta\left(\mathcal{A} + \frac{U_x^2}{4D_x} - \mathcal{H}\right)\Bigg] d\zeta \end{aligned} \tag{62}$$

$$\begin{aligned} \frac{\partial Q(t,x,y,z)}{\partial t} = & e^{-\mathcal{H}t} \int_0^t \Bigg\{ \left(\frac{\mathcal{B}\zeta}{t-\zeta}\right)^{\frac{1}{2}} I_1\left[2\left(\mathcal{B}\zeta(t-\zeta)\right)^{\frac{1}{2}}\right] \\ & - \mathcal{H} I_\circ\left[2\left(\mathcal{B}\zeta(t-\zeta)\right)^{\frac{1}{2}}\right]\Bigg\} \left(\frac{1}{4\pi D_z \zeta^3}\right)^{\frac{1}{2}} \\ & \times \exp\left[-\frac{1}{4\zeta}\left(\frac{x^2}{D_x} + \frac{y^2}{D_y} + \frac{z^2}{D_z}\right) - \zeta\left(\mathcal{A} + \frac{U_x^2}{4D_x} - \mathcal{H}\right)\right] d\zeta \\ & + e^{-\mathcal{H}t}\left(\frac{1}{4\pi D_z t^3}\right)^{\frac{1}{2}} \exp\Bigg[-\frac{1}{4t}\left(\frac{x^2}{D_x} + \frac{y^2}{D_y} + \frac{z^2}{D_z}\right) \\ & - t\left(\mathcal{A} + \frac{U_x^2}{4D_x} - \mathcal{H}\right)\Bigg] \end{aligned} \tag{63}$$

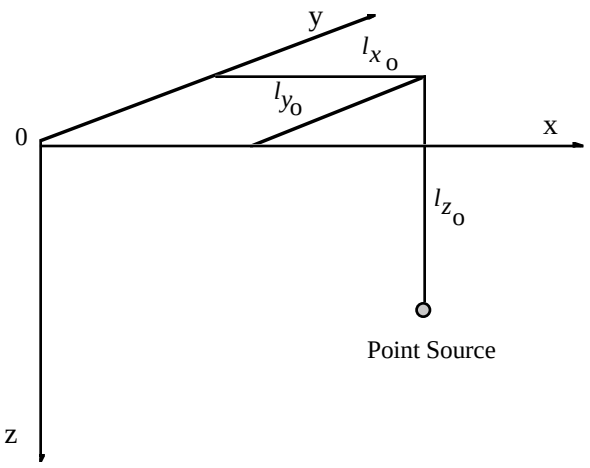

Figure 8. Schematic illustration of a virus point source with coordinates $\ell_{x_\circ}$, $\ell_{y_\circ}$, $\ell_{z_\circ}$

where I_1 is the modified Bessel function of the first kind of first order, and p, q and v are dummy integration variables.

Although the analytical solution (61)–(63) can be employed for point, two-, and three-dimensional source geometries, only a point source configuration described by the following mathematical expression is examined here

$$W(x, y, z) = \frac{1}{\theta}\delta(x - \ell_{x_\circ})\delta(y - \ell_{y_\circ})\delta(z - \ell_{z_\circ}) \tag{64}$$

where $-\infty < \ell_{x_\circ}, \ell_{y_\circ}, \ell_{z_\circ} < \infty$ represent x, y, z Cartesian coordinates of the virus point source, respectively, and δ is the Dirac delta function. A schematic illustration of a point source is shown in Figure 8.

3.1.1 Instantaneous virus loading

For instantaneous virus loading the mass release rate function is described by the following expression

$$G(t) = M\delta(t - t_\circ) \tag{65}$$

where M signifies the total virus mass released, and $t_\circ$ is the time of instantaneous virus release. In view of (64) and (65), the general solution (61) reduces to the analytical solution for the case of instantaneous virus loading conditions which is expressed as follows (Sim and Chrysikopoulos [48])

$$\begin{aligned} C(t,x,y,z) = \frac{M}{\theta} \int_0^{t-t_\circ} \left(\frac{1}{64\pi^3 D_x D_y D_z \zeta^3}\right)^{\frac{1}{2}} \Lambda_1(t-t_\circ) \\ \times \Lambda_2(t-t_\circ)\ \Lambda_3(\zeta, x-\ell_{x_\circ}, y-\ell_{y_\circ}, z-\ell_{z_\circ})\ d\zeta \\ + \frac{M}{\theta}\left(\frac{1}{64\pi^3 D_x D_y D_z (t-t_\circ)^3}\right)^{\frac{1}{2}} \Lambda_1(t-t_\circ) \\ \times \Lambda_3(t-t_\circ, x-\ell_{x_\circ}, y-\ell_{y_\circ}, z-\ell_{z_\circ}) \end{aligned} \tag{66}$$

where

$$\Lambda_1(t) = \exp\left[-\mathcal{H}t\right] \tag{67}$$

$$\Lambda_2(t) = \left(\frac{\mathcal{B}\zeta}{t-\zeta}\right)^{\frac{1}{2}} I_1\left[2\left(\mathcal{B}\zeta(t-\zeta)\right)^{\frac{1}{2}}\right] \tag{68}$$

$$\begin{aligned} \Lambda_3(t,x,y,z) = \exp\Bigg[\frac{U_x x}{2D_x} - \frac{1}{4t}\left(\frac{x^2}{D_x} + \frac{y^2}{D_y} + \frac{z^2}{D_z}\right) \\ - t\left(\mathcal{A} + \frac{U_x^2}{4D_x} - \mathcal{H}\right)\Bigg] \end{aligned} \tag{69}$$

3.1.2 Continuous or periodic virus loading

For the case of a continuous or temporally periodic virus loading, the mass release rate function can be represented by a generalized Fourier series (Hassani [49])

$$G(t) = \overline{\Omega} + \sum_{n=1}^{\infty} \Omega_n \exp\left[\frac{i2n\pi t}{t_p}\right] \tag{70}$$

where $\overline{\Omega}$ represents the mean value of the virus mass release rate from the source, Ω_n is a spectrum of known coefficients, n is the wave number, and t_p is the temporal period of fluctuation. It should be noted that for the special case of an infinite period ($t_p \rightarrow \infty$), (70) reduces to a constant rate source loading ($G = \overline{\Omega}$).

In view of (61), (64) and (70), the appropriate analytical solution for continuous/periodic virus loading conditions is given by (Sim and Chrysikopoulos [48])

$$\begin{aligned} C(t,x,y,z) = & \int_0^t \int_0^\tau \left(\frac{1}{64\pi^3 D_x D_y D_z \zeta^3} \right)^{\frac{1}{2}} \frac{G(t-\tau)}{\theta} \; \Lambda_1(\tau) \; \Lambda_2(\tau) \\ & \times \Lambda_3(\zeta, x-\ell_{x_\circ}, y-\ell_{y_\circ}, z-\ell_{z_\circ}) \; d\zeta \; d\tau \\ & + \int_0^t \left(\frac{1}{64\pi^3 D_x D_y D_z \tau^3} \right)^{\frac{1}{2}} \frac{G(t-\tau)}{\theta} \\ & \times \Lambda_1(\tau) \; \Lambda_3(\tau, x-\ell_{x_\circ}, y-\ell_{y_\circ}, z-\ell_{z_\circ}) \; d\tau \end{aligned} \tag{71}$$

3.1.3 Model simulations

For a continuous point source of viruses located at $\ell_{x_\circ}$=$\ell_{y_\circ}$=$\ell_{z_\circ}$=100 cm within a homogeneous, saturated aquifer, assuming that the colloid filtration theory is applicable, which implies that the conditions (18) and (19) are valid, the analytical solution (71) is employed to investigate the effect of the two different inactivation rate coefficients on suspended virus concentration. Virus breakthrough concentrations at a location with coordinates $x = 109$ cm and $y = z = 100$ cm, for three different inactivation rate coefficients for liquid phase (λ) and adsorbed (λ^*) viruses are presented in Figure 9. It should be noted that the concentration profiles are conveniently normalized by the steady state concentration in the absence of inactivation, evaluated at $t = 100$ d (C_∞) as suggested by Hunt [50]. It is shown that the liquid phase virus concentration decreases with increasing λ and λ^*. This result is intuitive because an increase in λ or λ^* implies an increase in the inactivation rate of liquid phase or sorbed viruses,

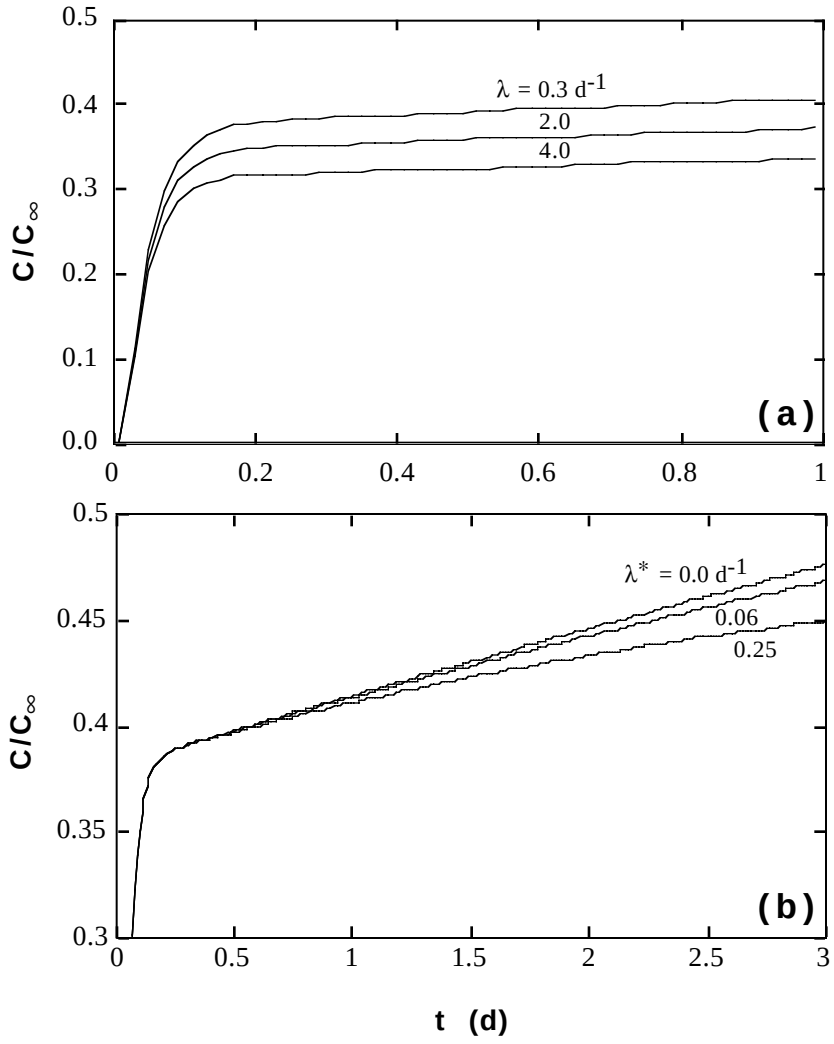

Figure 9. Effect of the inactivation rate coefficients for (a) liquid phase and (b) sorbed viruses on normalized breakthrough virus concentrations simulated by (71) under continuous virus loading conditions (here $D_x = 15$ cm^2/h, $D_y = D_z = 1.13$ cm^2/h, $U_x = 4$ cm/h, $t_\circ = 0$ d, $x = 109$ cm, $y = z = 100$ cm, $G = \overline{\Omega} = 1$ pfu/h, $k_c = 0.6$ h^{-1}, $k_r = 0.005$ h^{-1}, $\lambda = 0.25$ d^{-1}, and $\lambda^* = 0$ d^{-1}, $\theta = 0.25$ and $\rho = 1.5$ g/cm^3)

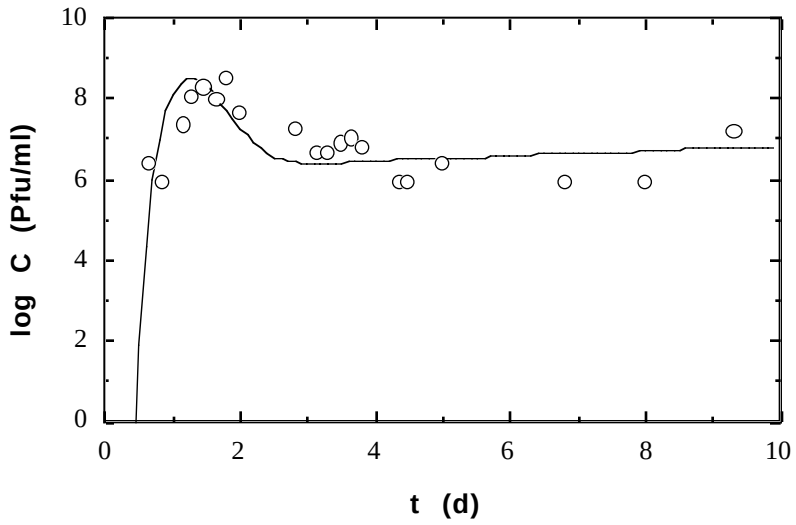

Figure 10. Bacteriophage PRD-1 normalized concentration breakthrough data (open circles) adopted from Bales *et al.* (1997) and simulated concentration history (solid curve) as predicted by (66)

respectively, and consequently a decrease in the concentration of suspended viruses.

The analytical solution applicable for a point source geometry under instantaneous loading conditions (66) was employed to simulate data from a bacteriophage PRD-1 transport experiment in a sandy aquifer in Borden, Ontario, Canada, reported by Bales *et al.* [51]. Bacteriophage PRD-1 is a virus that infects only certain strains of *Salmonella* bacteria. The field experiment was conducted with a point source geometry under instantaneous loading conditions. The field data used in this study were collected at monitoring well ML4-6. For simplicity, it was assumed that $\alpha_x/10 = \alpha_y = \alpha_z$, where α_x, α_y, and α_z are the longitudinal, lateral, and vertical dispersivities, respectively ($D_i = \alpha_i U_x, \quad i = x, y, z$). Given the experimental parameters $M = 1.24 \times 10^{13}$ pfu, $t_\circ = 0$ d, $U_x = 9$ cm/d, $x = 100.0$ cm, $\theta = 0.3$, $\lambda = \lambda^* = 0\ \mathrm{d}^{-1}$, and $\rho = 1.81\ \mathrm{g/cm^3}$, the values for $r_1 = 0.21$ h^{-1}, $r_2 = 0.0046\ \mathrm{g/cm^3 h}$, and $\alpha_x = 27.36$ cm were estimated by a

nonlinear least squares regression method (IMSL [38]). Figure 10 shows a good agreement between the simulated concentration history (solid line) and the bacteriophage PRD–1 experimental data (circles). The corresponding *sse* was estimated to be 8.76. In view of the estimated values for r_1 and r_2, the corresponding nonequilibrium sorption parameters $k = 0.21$ h^{-1} and $K_d = 46.19$ cm^3/g were calculated from (14) and (15), respectively, whereas the filtration parameters $k_c = 0.21$ h^{-1} and $k_r = 0.0008$ h^{-1} were calculated from (18) and (19), respectively. It should be noted that the estimated longitudinal dispersivity at ML4-6 ($\alpha_x = 27.36$ cm) is within the range of values (10–60 cm) obtained by Li [52] from electrical conductivity breakthrough curves.

3.2 Aquifer with semi-infinite thickness

The appropriate initial and boundary conditions for an aquifer with infinite longitudinal and lateral directions and semi-infinite vertical direction (thickness), as illustrated schematically in Figure 11, are as follows:

$$C(0, x, y, z) = 0 \tag{72}$$

$$C(t, \pm\infty, y, z) = 0 \tag{73}$$

$$C(t, x, \pm\infty, z) = 0 \tag{74}$$

$$\frac{\partial C(t, x, y, 0)}{\partial z} = 0 \tag{75}$$

$$\frac{\partial C(t, x, y, \infty)}{\partial z} = 0 \tag{76}$$

where the condition (72) corresponds to the situation in which viruses are initially absent from the three-dimensional porous formation, (73) and (74) indicate that the aquifer is infinite horizontally and laterally, boundary condition (75) represents a zero dispersive flux boundary, and (76) preserves concentration continuity for a semi-infinite vertical aquifer thickness. The vertical level $z = 0$ defines the location of the water table or a confining layer.

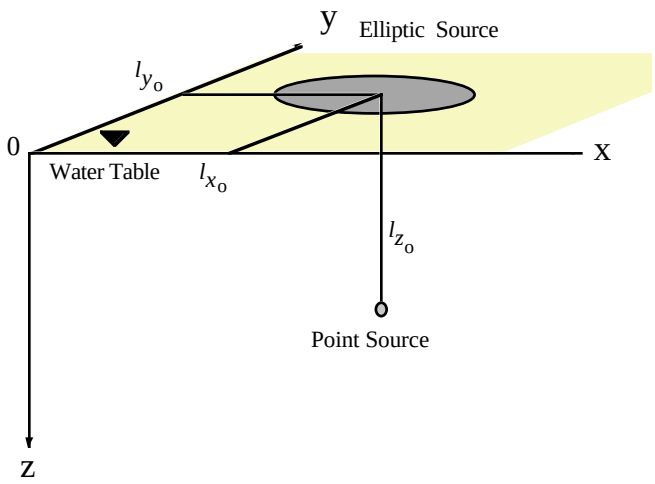

Figure 11. Schematic illustration of point and elliptic sources of virus contamination with coordinates $\ell_{x_\circ}$, $\ell_{y_\circ}$, $\ell_{z_\circ}$ in an aquifer with semi-infinite thickness. Note that the positive direction for the vertical coordinate is inverted

The analytical solution to the governing three-dimensional integrodifferential equation (55) subject to conditions (72)–(76) was derived by integral transform techniques by Sim and Chrysikopoulos [53] for a similar type of contaminant transport problem and is expressed as

$$C(t,x,y,z) = \left(\frac{1}{64\pi^3 D_x D_y D_z}\right)^{\frac{1}{2}} \int_0^t \int_{-\infty}^{\infty} \int_{-\infty}^{\infty} \int_0^{\infty} S(t-\tau,q,v,p)$$

$$\times \Psi_1(\tau)\left\{ \int_0^\tau \frac{\Psi_2(\tau)}{\zeta^{\frac{3}{2}}}\ \Psi_3(\zeta, x-q, y-v)\right.$$

$$\times \Big[\Psi_4(\zeta, z+p) + \Psi_4(\zeta, z-p)\Big]\ d\zeta$$

$$+ \frac{\Psi_3(\tau, x-q, y-v)}{\tau^{\frac{3}{2}}}$$

$$\left.\times \Big[\Psi_4(\tau, z+p) + \Psi_4(\tau, z-p)\Big]\right\}\ dp\ dv\ dq\ d\tau \qquad (77)$$

where

$$\Psi_1(t) = \exp\big[-\mathcal{H}t\big] \tag{78}$$

$$\Psi_2(t) = \left(\frac{\mathcal{B}\zeta}{t-\zeta}\right)^{\frac{1}{2}} I_1\Big[2\big(\mathcal{B}\zeta(t-\zeta)\big)^{\frac{1}{2}}\Big] \tag{79}$$

$$\Psi_3(t,x,y) = \exp\left[\frac{U_x x}{2D_x} - \frac{1}{4t}\left(\frac{x^2}{D_x} + \frac{y^2}{D_y}\right) - t\left(\mathcal{A} - \mathcal{H} + \frac{U_x^2}{4D_x}\right)\right] \tag{80}$$

$$\Psi_4(t,z) = \exp\left[\frac{-z^2}{4D_z t}\right] \tag{81}$$

The analytical solution (77) is quite general and can be employed for both point and circular/elliptic source geometries.

3.2.1 Point source geometry

For a point source configuration, in view of (56) and (64), the general analytical solution for virus transport in an aquifer with semi-infinite thickness, (77), reduces to the following expression

$$\begin{aligned} C(t,x,y,z) = \left(\frac{1}{64\pi^3 D_x D_y D_z}\right)^{\frac{1}{2}} \int_0^t \frac{G(t-\tau)}{\theta} \\ \times \Psi_1(\tau)\Bigg\{\int_0^\tau \frac{\Psi_2(\tau)}{\zeta^{\frac{3}{2}}}\ \Psi_3(\zeta, x-\ell_{x_\circ}, y-\ell_{y_\circ}) \\ \times \Big[\Psi_4(\zeta, z+\ell_{z_\circ}) + \Psi_4(\zeta, z-\ell_{z_\circ})\Big]\, d\zeta \\ + \frac{\Psi_3(\tau, x-\ell_{x_\circ}, y-\ell_{y_\circ})}{\tau^{\frac{3}{2}}} \\ \times \Big[\Psi_4(\tau, z+\ell_{z_\circ}) + \Psi_4(\tau, z-\ell_{z_\circ})\Big]\Bigg\}\, d\tau \end{aligned} \tag{82}$$

where $\Psi_1, \ldots, \Psi_4$ are defined in (78)–(81), respectively.

For instantaneous virus loading conditions, the mass release rate function $G(t)$ is defined by (65). For this special case, (82) reduces to the following expression suitable for virus transport with a point source geometry under instantaneous virus loading conditions in an aquifer with semi-infinite thickness

$$\begin{aligned} C(t,x,y,z) = & \left(\frac{1}{64\pi^3 D_x D_y D_z}\right)^{\frac{1}{2}} \frac{M}{\theta}\ \Psi_1(t-t_\circ) \\ & \times \left\{ \int_0^{t-t_\circ} \frac{\Psi_2(t-t_\circ)}{\zeta^{\frac{3}{2}}}\ \Psi_3(\zeta, x-\ell_{x_\circ}, y-\ell_{y_\circ}) \right. \\ & \times \Big[\Psi_4(\zeta, z+\ell_{z_\circ}) + \Psi_4(\zeta, z-\ell_{z_\circ})\Big]\ d\zeta \\ & + \frac{\Psi_3(t-t_\circ, x-\ell_{x_\circ}, y-\ell_{y_\circ})}{(t-t_\circ)^{\frac{3}{2}}} \\ & \left. \times \Big[\Psi_4(t-t_\circ, z+\ell_{z_\circ}) + \Psi_4(t-t_\circ, z-\ell_{z_\circ})\Big] \right\} \end{aligned} \quad (83)$$

3.2.2 Circular/elliptic source geometry

An elliptic source geometry can be described mathematically by the following expression

$$W(x,y,z) = \begin{cases} \dfrac{\delta(z-\ell_{z_\circ})}{\theta} & \dfrac{(x-\ell_{x_\circ})^2}{a^2} + \dfrac{(y-\ell_{y_\circ})^2}{b^2} \le 1 \\ 0 & \text{otherwise} \end{cases} \quad (84)$$

where $\ell_{x_\circ}$, $\ell_{y_\circ}$, $\ell_{z_\circ}$ are x, y, z Cartesian coordinates of the center of the elliptic source geometry, respectively, and a and b represent the semi-axes of the ellipse parallel to x- and y-axes, respectively. It should be noted that here G signifies the virus mass release rate per unit source area.

In view of (56) and (84), the general analytical solution (77) reduces to the following expression which is applicable to virus transport in a homogeneous, saturated aquifer with semi-infinite thickness and elliptic source geometry

$$C(t,x,y,z) = \left(\frac{1}{64\pi^2 D_x D_z}\right)^{\frac{1}{2}} \int_0^t \int_{a_1}^{a_2} \frac{G(t-\tau)}{\theta}$$
$$\times \Psi_1(\tau) \Bigg\{ \int_0^\tau \frac{\Psi_2(\tau)}{\zeta}\ \Psi_3(\zeta, x-q, 0)$$
$$\times \Big[\Psi_4(\zeta, z+\ell_{z_\circ}) + \Psi_4(\zeta, z-\ell_{z_\circ})\Big]\ \Psi_5(\zeta)\ d\zeta$$
$$+ \Big[\Psi_4(\tau, z+\ell_{z_\circ}) + \Psi_4(\tau, z-\ell_{z_\circ})\Big]\ \Psi_5(\tau)$$
$$\times \frac{\Psi_3(\tau, x-q, 0)}{\tau} \Bigg\}\ dq\ d\tau \tag{85}$$

where $\Psi_1, \ldots, \Psi_4$ are defined in (78)–(81), respectively,

$$\Psi_5(t) = \operatorname{erf}\Big[\mathcal{K}_1(t,q,y)\Big] - \operatorname{erf}\Big[\mathcal{K}_2(t,q,y)\Big] \tag{86}$$

$$a_1 = \ell_{x_\circ} - a \tag{87}$$

$$a_2 = \ell_{x_\circ} + a \tag{88}$$

$$\mathcal{K}_1(t,q,y) = \left\{ y - \ell_{y_\circ} + \left[b^2 - \frac{b^2 (q-\ell_{x_\circ})^2}{a^2} \right]^{\frac{1}{2}} \right\} \left(\frac{1}{4D_y t}\right)^{\frac{1}{2}} \tag{89}$$

$$\mathcal{K}_2(t,q,y) = \left\{ y - \ell_{y_\circ} - \left[b^2 - \frac{b^2 (q-\ell_{x_\circ})^2}{a^2} \right]^{\frac{1}{2}} \right\} \left(\frac{1}{4D_y t}\right)^{\frac{1}{2}} \tag{90}$$

and erf[ ] is the error function. As noted by Chrysikopoulos [54], solving for an elliptic source geometry is advantageous because the appropriate solution for a circular source can easily be obtained by setting $a = b = r$ in (87)–(90), where r is the radius of the circular source.

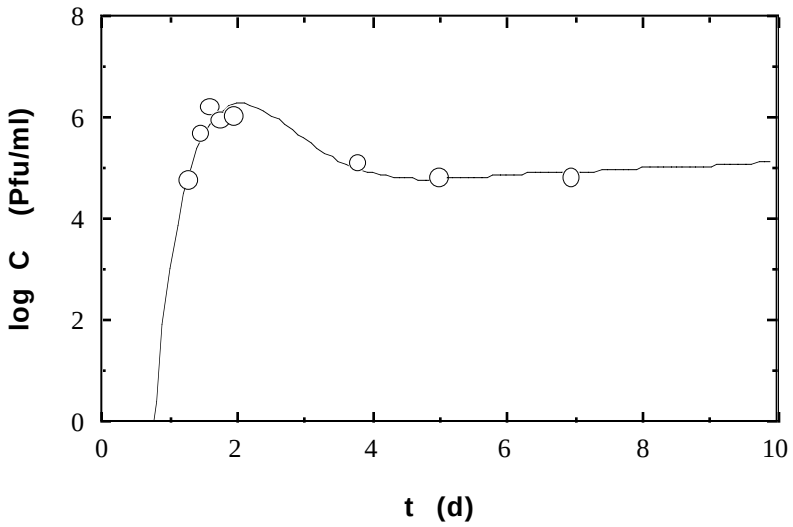

Figure 12. Bacteriophage M-1 breakthrough experimental data (open circles) adopted from Bales *et al.* [51] and simulated concentration history (solid curve) as predicted by (83)

3.2.3 Field application

The analytical solution applicable for virus transport originating from a point source under instantaneous virus loading conditions in semi-infinite porous media, (83), is employed to simulate data from a bacteriophage M–1 transport experiment in a sandy aquifer in Borden, Ontario, Canada, reported by Bales *et al.* [51]. The M–1 virus is a heat-resistant bacteriophage. The field data used in this study were collected at monitoring well ML4–6. Given the experimental parameters $M = 1.0 \times 10^{11}$ pfu, $t_\circ = 0$ d, $U_x = 9$ cm/d, $x = 100.0$ cm, $\theta = 0.3$, $\lambda = \lambda^* = 0$ d^{-1}, and $\rho = 1.81$ g/cm^3, the values for $r_1 = 0.105$ h^{-1}, $r_2 = 0.005$ g/cm^{3}h, were estimated by a nonlinear least squares regression method (IMSL [38]). The longitudinal dispersivity, $\alpha_x = 18.9$ cm, at ML4–6 was obtained from electrical conductivity breakthrough experiments conducted by Li [52, Table 6.4]. Figure 12 shows a very good agreement between the simulated

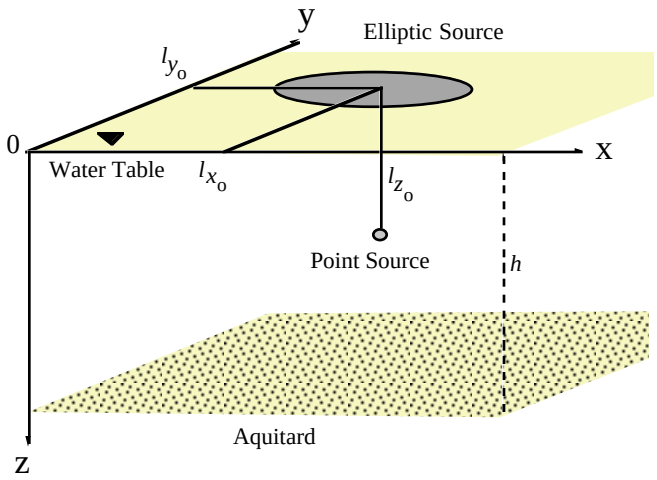

Figure 13. Schematic illustration of point and elliptic sources of virus contamination with coordinates $\ell_{x_\circ}$, $\ell_{y_\circ}$, $\ell_{z_\circ}$ in an aquifer with finite thickness. Note that the positive direction for the vertical coordinate is inverted

concentration history (solid line) and the bacteriophage M–1 experimental data (circles). The corresponding *sse* was estimated to be 0.29. In view of the estimated values for r_1 and r_2, the corresponding nonequilibrium sorption parameters $k = 0.105$ h^{-1} and $K_d = 20.83$ cm^3/g were calculated from (14) and (15), respectively, whereas the filtration parameters $k_c = 0.105$ h^{-1} and $k_r = 0.00084$ h^{-1} were calculated from (18) and (19), respectively.

3.3 Aquifer with finite thickness

For an aquifer with finite thickness, as illustrated schematically in Figure 13, the appropriate finite vertical, lower boundary condition, which implies that the aquifer is confined by an impermeable layer at depth $z = h$, is expressed as follows

$$\frac{\partial C(t, x, y, h)}{\partial z} = 0 \tag{91}$$

where h is the aquifer thickness. Following the work by Sim and Chrysikopoulos [53], the analytical solution of (55) subject to conditions (72)–(75) and (91) is given by

$$\begin{aligned} C(t,x,y,z) = \left(\frac{1}{16\pi^2 D_x D_y}\right)^{\frac{1}{2}} \int_0^t \int_{-\infty}^{\infty} \int_{-\infty}^{\infty} \Psi_1(\tau) \\ \times \left\{ \int_0^\tau \frac{\Psi_2(\tau)}{\zeta} \Psi_3(\zeta, x-q, y-v) \right. \\ \times \Psi_6\Big(\zeta, \ddot{S}(t-\tau,q,v,0), \ddot{S}(t-\tau,q,v,\psi_m)\Big)\, d\zeta \\ + \Psi_6\Big(\tau, \ddot{S}(t-\tau,q,v,0), \ddot{S}(t-\tau,q,v,\psi_m)\Big) \\ \left. \times \frac{\Psi_3(\tau, x-q, y-v)}{\tau} \right\} dv\ dq\ d\tau \end{aligned} \tag{92}$$

where $\Psi_1, \ldots, \Psi_3$ are defined in (78)–(80), respectively,

$$\Psi_6(t, f_1, f_2) = \frac{f_1}{h} + \frac{2}{h} \sum_{m=1}^{\infty} f_2 \exp\left[-\psi_m^2 D_z t\right] \cos\left(\psi_m z\right) \tag{93}$$

$$\psi_m = \frac{m\pi}{h} \tag{94}$$

m is the integer summation index, $\ddot{S}(t,x,y,\psi_m)$ represents the finite Fourier cosine transform of $S(t,x,y,z)$ with respect to space variable z with corresponding finite Fourier cosine transform variable ψ_m, and f_1 and f_2 are arbitrary functions.

3.3.1 Point source geometry

For a point source geometry, the general solution corresponding to the case of an aquifer with finite thickness (92) reduces to the following form (Sim and Chrysikopoulos [53])

$$C(t,x,y,z) = \left(\frac{1}{16\pi^2 D_x D_y}\right)^{\frac{1}{2}} \int_0^t \frac{G(t-\tau)}{\theta}\ \Psi_1(\tau) \left\{ \int_0^\tau \frac{\Psi_2(\tau)}{\zeta} \right.$$

$$\times \Psi_3(\zeta, x-\ell_{x_\circ}, y-\ell_{y_\circ})\ \Psi_6\left(\zeta, 1, \cos\left(\psi_m \ell_{z_\circ}\right)\right)\ d\zeta$$
$$+ \frac{\Psi_3(\tau, x-\ell_{x_\circ}, y-\ell_{y_\circ})}{\tau}\ \Psi_6\left(\tau, 1, \cos\left(\psi_m \ell_{z_\circ}\right)\right) \Bigg\} d\tau \quad (95)$$

where $\Psi_1, \ldots, \Psi_3$ and Ψ_6 are defined in (78)–(80) and (93), respectively.

3.3.2 Elliptic source geometry

For an elliptic source geometry the general solution corresponding to the case of an aquifer with finite thickness (92) reduces to the following form (Sim and Chrysikopoulos [53])

$$C(t,x,y,z) = \left(\frac{1}{16\pi D_x}\right)^{\frac{1}{2}} \int_0^t \int_{a_1}^{a_2} \frac{G(t-\tau)}{\theta}\ \Psi_1(\tau) \Bigg\{ \int_0^\tau \frac{\Psi_2(\tau)}{\zeta^{\frac{1}{2}}}$$
$$\times \Psi_3(\zeta, x-q, 0)\ \Psi_5(\zeta)\ \Psi_6\left(\zeta, 1, \cos\left(\psi_m \ell_{z_\circ}\right)\right) d\zeta$$
$$+ \frac{\Psi_3(\tau, x-q, 0)}{\tau^{\frac{1}{2}}} \Psi_5(\tau) \Psi_6\left(\tau, 1, \cos\left(\psi_m \ell_{z_\circ}\right)\right) \Bigg\} dq\ d\tau \quad (96)$$

where a_1 and a_2 are defined in (87) and (88), respectively, and $\Psi_1, \ldots, \Psi_3$, Ψ_5, and Ψ_6 are defined in (78)–(80), (86), and (93), respectively.

4 Summary

One- and three-dimensional analytical models for virus transport in saturated, homogeneous porous media were presented. The virus transport models considered in this chapter account for first-order inactivation of liquid phase and deposited viruses with different inactivation rate coefficients, and virus attachment onto the solid matrix of the porous formation by either nonequilibrium adsorption or modified colloid filtration. The three-dimensional virus transport models

are applicable to aquifers with either semi-infinite or finite thickness and can accommodate a variety of source loadings and virus source geometries. The analytical solutions presented here are particularly useful for preliminary estimation of virus migration, characterization of virus contamination sources, examination of possible aquifer boundary conditions, validation of numerical solutions, and determination of virus transport parameters from laboratory or well defined field experiments. However, the applicability of the analytical solutions presented here is limited to homogeneous subsurface formations. It should be noted that multidimensional contaminant transport models are more advantageous than one-dimensional models, because they can account for concentration gradients and contaminant transport in directions perpendicular to the groundwater flow. Furthermore, multidimensional models can easily account for a variety of boundary conditions as well as contaminant source geometries.

Acknowledgments

The preparation of this chapter was supported in part jointly by the National Water Research Institute and the University of California, Water Resources Center, as part of Water Resources Center Projects UCAL–WRC–854 and UCAL–WRC–890. The content of this manuscript does not necessarily reflect the views of the agencies and no official endorsement should be inferred.

Notation

a	semi-axis of the elliptic source parallel to x-axis, L.
a_t	time correlation scale of K'_d, t.
a_1, a_2	defined in (87) and (88), respectively.
A	defined in (40).
$\mathcal{A}$	defined in (8a), t^{-1}.
b	semi-axis of the elliptic source parallel to y-axis, L.
b°	constant related to the bonding energy, L^3/M.
B	defined in (41).
$\mathcal{B}$	defined in (8b), t^{-2}.

C	liquid phase virus concentration, M/L^3.
$C_\circ$	source concentration, M/L^3.
C^*	sorbed virus concentration (virus mass/solid mass), M/M.
C_g	concentration of virus directly in contact with solids, M/L^3.
C_∞	steady state virus concentration in the absence of inactivation, M/L^3.
D_x	longitudinal hydrodynamic dispersion coefficient, L^2/t.
D_y	lateral hydrodynamic dispersion coefficient, L^2/t.
D_z	vertical hydrodynamic dispersion coefficient, L^2/t.
erf$[\eta]$	error function, equal to $(2/\pi^{\frac{1}{2}}) \int_0^\eta e^{-\zeta^2} d\zeta$.
erfc$[\eta]$	complimentary error function, equal to $(2/\pi^{\frac{1}{2}}) \int_\eta^\infty e^{-\zeta^2} d\zeta$.
$E[\ ]$	expectation operator.
$\mathcal{E}$	relative mass balance error, defined in (20).
f_1, f_2	arbitrary functions.
F	defined in (35).
G	virus source loading function, M/t.
$\mathcal{G}$	defined in (39).
h	finite aquifer thickness, L.
H	defined in (42).
$\mathcal{H}$	defined in (8c), t^{-1}.
$I_\circ[\ ]$	modified Bessel function of the first kind of zeroth order.
$I_1[\ ]$	modified Bessel function of the first kind of first order.
$J_\circ[\ ]$	Bessel function of the first kind of zeroth order.
k	mass transfer rate constant, t^{-1}.
k_c	clogging rate constant, t^{-1}.
k_r	declogging rate constant, t^{-1}.
k_1	forward reaction rate, t^{-1}.
k_2	reverse reaction rate, t^{-1}.
K_d	partition or distribution coefficient, L^3/M.
K_d'	zero-mean random fluctuation of $\langle K_d \rangle$, L^3/M.
$\mathcal{K}_1, \mathcal{K}_2$	defined in (89) and (90), respectively.
ℓ	characteristic or reference length, L.
$\ell_{i_\circ}$	Cartesian coordinates of a virus point source or the center of a circular/elliptic source ($i = x, y, z$), L.
m	integer summation index.
M	total virus mass released into the porous formation, M.
n	wave number.
p	dummy integration variable.

Pe Peclet number, equal to $U_x \ell / D_x$.
q dummy integration variable.
Q defined in (62).
Q_1, Q_2 defined in (43) and (44), respectively.
Q° Langmuir monolayer capacity, M/M.
r radius of circular source, L.
r_1 forward rate coefficient, t^{-1}.
r_2 reverse rate coefficient, $\mathrm{M/L^3}t$.
S virus source configuration, $\mathrm{M/L^3t}$.
$\ddot{S}$ finite Fourier cosine transform of S.
t time, t.
$t_\circ$ arbitrary time, t.
t_p temporal period, t.
U_x average interstitial velocity, L/t.
v dummy integration variable.
W virus source geometry function, L^{-3}.
x, y, z spatial coordinates in the longitudinal, lateral, and vertical direction, respectively, L.
$\langle\ \rangle$ expected value, equivalent to $E[\ ]$.

Greek letters

α resistivity coefficient of viruses in the liquid phase, t^{-1}.
α^* resistivity coefficient of sorbed viruses, t^{-1}.
α_x longitudinal dispersivity, L.
α_y lateral dispersivity, L.
α_z vertical dispersivity, L.
$\delta(\ )$ Dirac delta function.
ϵ fractional void volume, $\mathrm{L^3/L^3}$.
ζ dummy integration variable.
η arbitrary argument.
θ porosity (liquid volume/porous medium volume), $\mathrm{L^3/L^3}$.
κ defined in (46).
λ inactivation rate coefficient of suspended viruses, t^{-1}.
λ^* inactivation rate coefficient of sorbed viruses, t^{-1}.
$\lambda_\circ$ initial inactivation rate coefficient of suspended viruses, t^{-1}.
$\lambda_\circ^*$ initial inactivation rate coefficient of sorbed viruses, t^{-1}.
Λ defined in (48).
Λ_1–Λ_3 defined in (67)–(69), respectively.
ξ dummy integration variable.

ρ	bulk density of the solid matrix, M/L^3.
$\sigma^2_{K'_d}$	variance of K'_d.
τ	dummy integration variable.
ϕ	filter coefficient, L^{-1}.
ψ	defined in (33).
ψ_m	finite Fourier cosine transform variable with respect to spatial coordinate z, defined in (94).
Ψ_1–Ψ_4	defined in (78)–(81), respectively.
Ψ_5, Ψ_6	defined in (86) and (93), respectively.
ω	defined in (47).
Ω_n	spectrum of known coefficients, M/t.
$\overline{\Omega}$	mean virus mass release rate, M/t.

Subscripts

cc	constant concentration boundary condition.
cf	constant flux boundary condition.

Abbreviations

pfu	plaque-forming units.
sse	sums of squared error.

References

[1] Yates, M. V., S. R. Yates, J. Wagner, and C. P. Gerba, Modeling virus survival and transport in the subsurface, *J. Contamin. Hydrol.*, **1**, 329–345, 1987.

[2] Brock, T. D., and M. T. Madigan, *Biology of Microorganisms*, 6th ed., Prentice Hall, Englewood Cliffs, NJ, 874 pp., 1991.

[3] Gerba, C. P., and B. H. Keswick, Survival and transport of enteric bacteria and viruses in groundwater, *Stud. Environ. Sci.*, **17**, 511–515, 1981.

[4] Yates, M. V., and S. R. Yates, Modeling microbial fate in the subsurface environment, *Crit. Rev. Environ. Control*, **17**(4), 307–344, 1988.

[5] Vilker, V. L., Simulating virus movement in soils, in *Modeling Waste Renovation: Land Treatment*, edited by I. K. Iskandar, pp. 223–253, John Wiley, New York, 1981.

[6] Hurst, C. J., C. P. Gerba, and I. Cech, Effects of environmental variables and soil characteristics on virus survival in soil, *Appl. Environ. Microb.*, **40**, 1067–1079, 1980.

[7] Gerba, C. P., Applied and theoretical aspects of virus adsorption to surfaces, *Adv. Appl. Micrb.*, **30**, 133–168, 1984.

[8] Sobsey, M. D., C. H. Dean, M. E. Knuckles, and R. A. Wagner, Interaction and survival of enteric viruses in soil materials, *Appl. Environ. Microb.*, **40**, 92–101, 1980.

[9] Yates, M. V., and Y. Ouyang, VIRTUS, a model of virus transport in unsaturated soils, *Appl. Environ. Microb.*, **58**(5), 1609–1616, 1992.

[10] Park, N., T. N. Blanford, and P. S. Huyakorn, VIRALT: A modular semi-analytical and numerical model for simulating viral transport in ground water, Int. Ground Water Model. Cent., Colo. Sch. of Mines, Golden, 1992.

[11] Teutsch, G., K. Herbold-Paschke, D., Tougianidou, T. Hahn, and K. Botzenhart, Transport of microorganisms in the underground-processes, experiments, and simulation models, *Water Sci. Technol.*, **24**(2), 309–314, 1991.

[12] Powelson, D. K., and C. P. Gerba, Virus removal from sewage effluents during saturated and unsaturated flow through soil columns, *Water Res.*, **28**(10), 2175–2181, 1994.

[13] Gerba, C. P., M. V. Yates, and S. R. Yates, Quantization of factors controlling viral and bacterial transport in subsurface, in *Modeling the Environmental fate of Microorganisms*, American Society of Microbiology, Washington, DC, 1991.

[14] Powelson, D. K., C. P. Gerba, and M. T. Yahya, Virus transport and removal in wastewater during aquifer recharge, *Water Res.*, **27**(4), 583–590, 1993.

[15] Abdel-Salam, A., and C. V. Chrysikopoulos, Modeling of colloid and colloid-facilitated contaminant transport in a two-dimensional fracture with spatially variable aperture, *Transp. Porous Media*, **20**(3), 197-221, 1995.

[16] Chrysikopoulos, C. V., and A. Abdel-Salam, Modeling of colloid transport and deposition in saturated fractures, *Colloids Surfaces A: Physicochem. Eng. Aspects*, **121**, 189–202, 1997.

[17] Harvey, R. W., and S. P. Garabedian, Use of colloid filtration theory in modeling movement of bacteria through a contaminated sandy aquifer, *Env. Sci. Technol.*, **25**(1), 178–185, 1991.

[18] Matthess, G., A. Pekdeger, and J. Schroeter, Persistence and transport of bacteria and viruses in groundwater: A conceptual evaluation, *J. Contamin. Hydrol.*, **2**, 171–188, 1988.

[19] Tim, U. S., and S. Mostaghimi, Model for predicting virus movement through soils, *Ground Water*, **29**(2), 251–259, 1991.

[20] Grosser, P. W., A one-dimensional mathematical model of virus transport, Paper presented at the 2nd Int. Conf. on Ground-Water Quality Research, Okla., State Univ., Tulsa, Okla., March 26–29, 1984.

[21] Sim, Y., and C. V. Chrysikopoulos, Analytical models for one-dimen- sional virus transport in saturated porous media, *Water Resour. Res.*, **31**(5), 1429–1437, 1995. (Correction, *Water Resour. Res.*, **32**(5), 1473, 1996.)

[22] Abramowitz, M., and I. A. Stegun, *Handbook of Mathematical Functions*, 1046 pp., Dover, Mineola, N. Y., 1972.

[23] Lapidus, L., and N. R. Amundson, Mathematics of adsorption in beds, VI, The effect of longitudinal diffusion in ion exchange and chromatographic columns, *J. Phys. Chem.*, **56**, 984–988, 1952.

[24] van Genuchten, M. Th., and J. C. Parker, Boundary conditions for displacement experiments through short laboratory soil columns, *Soil Sci. Soc. Am. J.*, **48**, 703–708, 1984.

[25] Batu, V., and M. Th. van Genuchten, First- and third-type boundary conditions in two dimensional solute transport modeling, *Water Resour. Res.*, **26**(2), 339–350, 1990.

[26] Leij, F. J., T. H. Skaggs, and M. Th. van Genuchten, Analytical solutions for solute transport in three-dimensional semi-infinite porous media, *Water Resour. Res.*, **27**(10), 2719–2733, 1991.

[27] Abdel-Salam, A., and C. V. Chrysikopoulos, Analytical solutions for one-dimensional colloid transport in saturated fractures, *Adv. Water Resour.*, **17**, 283–296, 1994.

[28] Bales, R. C., S. R. Hinkle, T. W. Kroeger, and K. Stocking, Bacteriophage adsorption during transport through porous media: Chemical perturbations and reversibility, *Environ. Sci. Technol.,* **25**(12), 2088–2095, 1991.

[29] Kahaner, D., C. Moler, and S. Nash, *Numerical Methods and Software*, Prentice Hall, Englewood Cliffs, NJ, 1989.

[30] Parkinson, J. S., and R. J. Huskey, Deletion mutants of Bacteriophage Lambda, 1, Isolation and initial characterization, *J. Mol. Biol.*, **56**, 369–384, 1971.

[31] Pollard, E. C., and W. Solosko, The thermal inactivation of T_4 and λ Bacteriophage, *Biophys. J.*, **11**, 66–74, 1971.

[32] Yamagishi, H., and H. Ozeki, Comparative study of thermal inactivation of phage ϕ80 and Lambda, *Virology*, **48**, 316–322, 1972.

[33] Grant, S. B., E. J. List, and M. E. Lidstrom, Kinetic analysis of virus adsorption and inactivation in batch experiments; virus

adsorption, virus inactivation, equilibrium isotherms, *Water Resour. Res.*, **29**(7), 2067–2085, 1993.

[34] Chrysikopoulos, C. V., and Y. Sim, One-dimensional virus transport in homogeneous porous media with time-dependent distribution coefficient, *J. Hydrol.*, **185**, 199–219, 1996.

[35] Crane, S. R., and J. A. Moore, Modeling enteric bacterial die-off: A review, *Water, Air, Soil Pollut.*, **27**, 411–439, 1986.

[36] Sim, Y., and C. V. Chrysikopoulos, One-dimensional virus transport in porous media with time dependent inactivation rate coefficients, *Water Resour. Res.*, **32**(8), 2607–2611, 1996.

[37] Reddy, K. R., R. Khaleel, and M. R. Overcash, Behavior and transport of microbial pathogens and indicator organisms in soils treated with organic wastes, *J. Environ. Qual.*, **10**(3), 255–266, 1981.

[38] International Mathematics and Statistics Libraries, Inc., *IMSL MATH LIBRARY User's manual*, ver. 2.0, Houston, Tex., 1991.

[39] Durant, M. G., and P. V. Roberts, Spatial variability of organic solute sorption in the Borden aquifer, Tech. Report 303, Department of Civil Engineering, Stanford University, Stanford, CA, 1986.

[40] Bosma, W. J. P., A. Bellin, S. E. A. T. M. van der Zee, and A. Rinaldo, Linear equilibrium adsorbing solute transport in physically and chemically heterogeneous porous formations, 2, Numerical results, *Water Resour. Res.*, **29**(12), 4031–4043, 1993.

[41] Smith, D. W., R. K. Rowe, and J. R. Booker, The analysis of pollutant migration through soil with linear hereditary time-dependent sorption, *Int. J. Numer. Anal. Meth. Geomech.*, **17**, 255–274, 1993.

[42] Moody, J. B., Radionuclide migration/retardation: Research and development technology status report, Office of Nuclear Waste Isolation, Battelle Memorial Inst., ONWI–321, Springfield, VA, 61 pp., 1982.

[43] Vilker, V. L., and W. D. Burge, Adsorption mass transfer model for virus transfer in soils, *Water Res.*, **14**, 783–790, 1980.

[44] Norde, W., Adsorption of proteins from solution at the solid-liquid interface, *Adv. Colloid Interface Sci.*, **25**, 267–340, 1986.

[45] Agterberg, F. P., *Geomathematics*, Elsevier, The Netherlands, 596 pp., 1974.

[46] Chrysikopoulos, C. V., P. K. Kitanidis, and P. V. Roberts, Analysis of one-dimensional solute transport through porous media

with spatially variable retardation factor, *Water Resour. Res.*, **26**(3), 437–446, 1990.

[47] Bellin, A., A. Rinaldo, W. J. P. Bosma, S. E. A. T. M. van der Zee, and Y. Rubin, Linear equilibrium adsorbing solute transport in physically and chemically heterogeneous porous formations, 1, Analytical solutions, *Water Resour. Res.*, **29**(12), 4019–4030, 1993.

[48] Sim, Y., and C. V. Chrysikopoulos, Three-dimensional analytical models for virus transport in saturated porous media, *Transp. Porous Media*, **30**, 87–112, 1998.

[49] Hassani, S., *Foundations of Mathematical Physics*, Allyn and Bacon, Boston, 1991.

[50] Hunt, B., Dispersive sources in uniform groundwater flow, *J. Hydraul. Div. Am. Soc. Civ. Eng.*, **104**(HY1), 75–85, 1978.

[51] Bales, R. C., S. Li, T.-C. J. Yeh, M. E. Lenczewski, and C. P. Gerba, Bactriophage and microsphere transport in saturated porous media: Forced-gradient experiment at Borden, Ontario, *Water Resour. Res.*, **33**(4), 639–648, 1997.

[52] Li, S., Modeling biocolloid transport in saturated porous media, Ph.D. Dissertation, Univ. of Arizona, Tucson, 1993.

[53] Sim, Y., and C. V. Chrysikopoulos, Analytical solutions for solute transport in saturated porous media with semi-infinite or finite thickness, *Adv. Water Resour.*, **22**(5), 507–519, 1999.

[54] Chrysikopoulos, C. V., Three-dimensional analytical models of contaminant transport from nonaqueous phase liquid pool dissolution in saturated subsurface formations, *Water Resour. Res.*, **31**(4), 1137–1145, 1995.